LA-UR- 09-06459

Approved for public release; distribution is unlimited.

Title:	Modeling the Viscoplastic Micromechanical Response of Two-Phase Materials using Fast Fourier Transforms
Author(s):	Sukbin Lee, Anthony D. Rollett, Ricardo A. Lebensohn
Intended for:	International Journal of Plasticity

Form 836 (7/06)

Modeling the Viscoplastic Micromechanical Response of Two-Phase Materials using Fast Fourier Transforms

S.-B. Lee [a,1], R. A. Lebensohn [b], and A. D. Rollett [a,1]

[a] *Department of Materials Science and Engineering, Carnegie Mellon University, Pittsburgh, PA 15213, U.S.A.*
[b] *Materials Science and Technology Division, Los Alamos National Laboratory, Los Alamos, NM 87845, USA*

Abstract

A viscoplastic approach using the Fast Fourier Transform (FFT) method for obtaining local mechanical response is utilized to study microstructure-property relationships in composite materials. Specifically, three-dimensional, two-phase digital materials containing isotropically coarsened particles surrounded by a matrix phase, generated through a Kinetic Monte Carlo Potts model for Ostwald ripening, are used as instantiations in order to calculate the stress and strain rate fields under uniaxial tension. The effects of the morphology of the matrix phase, the volume fraction and the contiguity of particles, and the polycrystallinity of matrix phase, on the stress and strain rate fields under uniaxial tension are examined. It is found that the first moments of the stress and strain rate fields have a different dependence on the particle volume fraction and the particle contiguity from their second moments. The average stresses and average strain rates of both phases and of the overall composite have rather simple relationships with the particle volume fraction whereas their standard deviations vary strongly, especially when the particle volume fraction is high, and the contiguity of particles has a noticeable effect on the mechanical response. It is also found that the shape of stress distribution in the BCC hard particle phase evolves as the volume fraction of particles in the composite varies, such that it agrees with the stress field in the BCC polycrystal as the volume of particles approaches unity. Finally, it is observed that the stress and strain rate fields in the microstructures with a polycrystalline matrix are less sensitive to changes in volume fraction and contiguity of particles.

Keywords: Micromechanical Modeling; Composite materials; Stress and strain rate fields; Viscoplasticity; Microstructure-property relationship

1. Introduction

It is well known in Materials Science that the properties of materials are a function of their microstructural parameters. In studying microstructure-property relationships, it is crucial to map the microstructural parameters obtained from materials

[1] Corresponding author. Tel: 1 412 268 3177
E-mail address: rollett@andrew.cmu.edu (A. D. Rollett)
[1] *Current address: School of Materials Engineering, Purdue University, 501 Northwestern Avenue, West Lafayette, In 47907-2044, USA*
E-mail address: lee797@purdue.edu (S.-B. Lee)

characterization to the desired materials property. Conventionally, materials characterization is based on data obtained from two-dimensional plane sections because of the opacity of most crystalline materials. However, many problems related to the properties of materials are three-dimensional in nature (Becker and Panchanadeeswaran, 1995; Lin et al., 1995; Patton et al., 1998; Shan and Gokhale, 2001; Suresh, 1998) because most materials of technological relevance have a polycrystalline or multi-phase structure with significant complexity in the spatial arrangement of their microstructural units. Even though stereology (Underwood, 1970) can be used to deduce the three-dimensional microstructure from conventional two-dimensional characterization, its statistical approach inevitably requires various spatial and morphological assumptions about the structural units. For example, even though the contiguity of particles can be easily measured in two-dimensional sections, it is hard to deduce three-dimensional particle contiguity from those two-dimensional observations without significant assumptions about particle shapes and spatial distribution.

In order to estimate three-dimensional microstructural features of materials directly, one can use the serial-sectioning methods (Morawiec and Saylor, 1999; Rollett et al., 2007; Rowenhorst et al., 2006a; Rowenhorst et al., 2006b; Saylor et al., 2002; Saylor et al., 2004; Tewari and Gokhale, 2001; Uchic et al., 2006). While this approach gives actual data on various microstructural parameters, one might need to reconstruct a number of samples of materials in order to use them as input for three-dimensional microstructure-property relationship studies, depending on the microstructural scale. In addition, in order to assess the effect of the individual microstructural parameters on the desired property, the samples must be prepared before the reconstruction process such that a specific microstructural feature is well controlled while the others remain constant. Naturally, this is difficult to perform and inefficient.

Alternatively, numerical simulations can be used for studying microstructure-property relationships. Especially for composite materials, unit cell models, solved numerically by means of the finite element method, have been used to calculate elastic and/or plastic behaviors of two-phase composites in either two- or three-dimensions (Chawla et al, 2006; Chawla and Chawla, 2006; Llorca et al., 1991; Shen et al., 1994). However, in those approaches, the geometry of the particles is, again, assumed to be simple and the representative unit cell is not able to capture the real microstructural complexities, which makes it impossible to compare the results directly to the experimental observations. Also, the model is not capable of explaining the long-range effect of the morphology of the matrix on the mechanical response of the materials.

In order to overcome these limitations, a microstructure-based modeling using serial sectioning method has been employed to investigate the deformation behavior of particle-reinforced composites (Chawla et al, 2006a; Chawla et al, 2006b; Chawla and Chawla, 2006). In these studies, the predictions of stress-strain relations under uniaxial tension from various types of microstructures (three-dimensional microstructures from serial sectioning, unit cell models with spherical, ellipsoidal or rectangular prismatic particles, and three-dimensional microstructures with spherical or ellipsoidal multi-particles) were compared to the result from experiments. It was found that the result from three-dimensional microstructure-based finite element model using serial sectioning method matches well with the experimental findings in terms of stress-strain curve since the shape and spatial distribution of the second phase particles in the reconstructed

microstructures are not arbitrarily assumed and modified. One interesting result, however, was that the plastic strain distribution from two-dimensional finite-element modeling is different from that in the two-dimensional section of the three-dimensional reconstructed microstructure-based one (Chawla et al., 2004; Chawla and Chawla, 2006) such that the regions in the matrix where the particles are sparsely spaced in the sections of the three-dimensional microstructure do not always experience the high plastic strain while it seemed to be always true in the two-dimensional modeling. Unfortunately, in many numerical simulation studies on two/three-dimensional particle-reinforced composites, including the works mentioned so far, the first moments of the effective mechanical fields (stress vs. elastic/plastic strain behavior) has been extensively analyzed with or without the consideration of microstructural effect on the mechanical fields (for example, see Batra and Love, 2006; Liu and Hu, 2005; Mercier and Moinari, 2009; Pierard et al., 2007; Vena et al., 2008). Also, to our best knowledge, there are few numerical studies on the mechanical response of the three-dimensional composite materials in terms of both the first and second moment analysis as a function of the microstructural parameters such as the volume fraction, the average size and the contiguity of particles, spatial orientations of two phases and the polycrystallinity of the matrix phase.

Given the facts and issues mentioned above, one way to meet the above challenges might be as follows: 1) develop numerical methods to generate hypothetical digital composite microstructures of whose representativity can be validated by comparison with the available experimental data; 2) measure the three-dimensional microstructural parameters of those hypothetical composite microstructures; and 3) use them as input for property simulation. Having measured the microstructural parameters from a representative three-dimensional digital microstructure, a property simulation model can be used to evaluate which combination of the microstructural parameters results in the desired mechanical state of the material for a given external load. In this work, we examine the stress and strain rate distributions in hypothetical composite microstructures under uniaxial tension, while varying certain microstructural parameters. To do this, we use a Fast Fourier Transform (FFT)-based algorithm (Lebensohn, 2001; Lebensohn et al., 2008; Lebensohn et al., 2009; Michel et al., 2000; Moulinec and Suquet, 1994; Moulinec and Suquet, 1998). This novel fast numerical method was originally proposed by Suquet and co-workers (Michel et al., 2000; Moulinec and Suquet, 1994; Moulinec and Suquet, 1998) to calculate the mechanical properties of two-dimensional materials based on pixellated microstructural data. While these authors first developed the method to calculate the mechanical behavior of two-phase isotropic composites, Lebensohn and co-authors (2001, 2008, 2009) applied their scheme to obtain the local response of the anisotropic polycrystals in the context of viscoplasticity. The FFT-based formulation provides an exact full-field solution of the governing equations and is used here to calculate the viscoplastic response of composite structures. The method, however, is limited to simulation cells with periodic boundary conditions. Here, we narrow the scope of our study to digitally generated two-phase composite materials, having an ensemble of isotropically coarsened particles wetted by a matrix phase (Lee et al., 2007) and apply uniaxial tension to them to explore their local response in terms of stress and strain rate fields.

Full-field solutions for stress and strain rate fields under uniaxial tension are calculated for two-phase anisotropic composite microstructures derived from Potts model simulations (Lee et al., 2007). The local heterogeneity is due to both particles and matrix phase being anisotropic with their stress-strain behavior given by the rate-sensitivity approach to crystal plasticity. The actual material that motivated this investigation is a liquid-phase sintered W-Ni-Fe, which has nearly pure W particles in a Ni-Fe based matrix, which also has some W dissolved in it (Fang and Patterson, 1993; Park et al., 1989; Tewari and Gokhale, 2001). Accordingly, isotropically coarsened particles in the simulated microstructures are assigned properties compatible with the harder body-centered cubic (BCC) structure with random orientations while the matrix phase is assigned properties associated with the softer face-centered cubic (FCC) structure.

The plan of the paper is as follows. In Section 2, we briefly review the numerical procedure for generating digital composite materials and define the microstructural parameters of interest. In Section 3, we discuss the FFT viscoplasticiy model as applied to composite materials. In Section 4, we investigate the relationship between the microstructural parameters and the predicted stress and strain rate fields. Finally, in Section 5, we close with some concluding remarks.

2. Preparation of input digital composite materials for property simulation

2.1. Generation of three-dimensional digital composites using Monte Carlo Potts model

A complete description of the simulations of Ostwald ripening (Lifshitz and Slyozov, 1961; Ostwald, 1900) used to generate three-dimensional digital composite microstructures containing an ensemble of isotropically coarsened particles with size variation, surrounded by a fully wetting matrix phase has been described in detail elsewhere (Lee et al., 2007). Accordingly, here we only highlight a few essential results of that work, in which it was reported that: 1) a fully-wetting condition by matrix phase is verified by observing the compact shape of the individual particles and the percolating spatial distribution of the matrix phase; 2) the final particle size distribution as a function of both volume fraction of particles and initial particle size distribution is in good agreement with typical ones found in experiments and it attains a statistical steady-state; and 3) the associated kinetics are consistent with theories of Ostwald ripening (Lifshitz and Slyozov, 1961; Ostwald, 1900).

During coarsening simulation, the matrix phase is defined as a collection of voxels with a same "spin" number, in order to represent the surrounding liquid medium through which the solid voxels can diffuse, making the ensemble of particles evolve. In that context, the matrix phase can be treated as a single crystal. In reality, however, the matrix phase after liquid phase sintering is polycrystalline at room temperature. Based on our ability to generate ensembles of isotropically coarsened particles that are representative of those in real composite systems from Ostwald ripening, we also generated a polycrystalline matrix in each microstructure. For simplicity, the Monte Carlo isotropic grain growth model (Anderson et al., 1985; Anderson et al., 1989; Srolovitz et al., 1983) was adopted to generate a polycrystalline matrix while the particles from coarsening simulation remain intact. Fig. 1 shows the particles ((a) and (b)) from coarsening simulation, the corresponding single crystal matrix ((c) and (d)), and

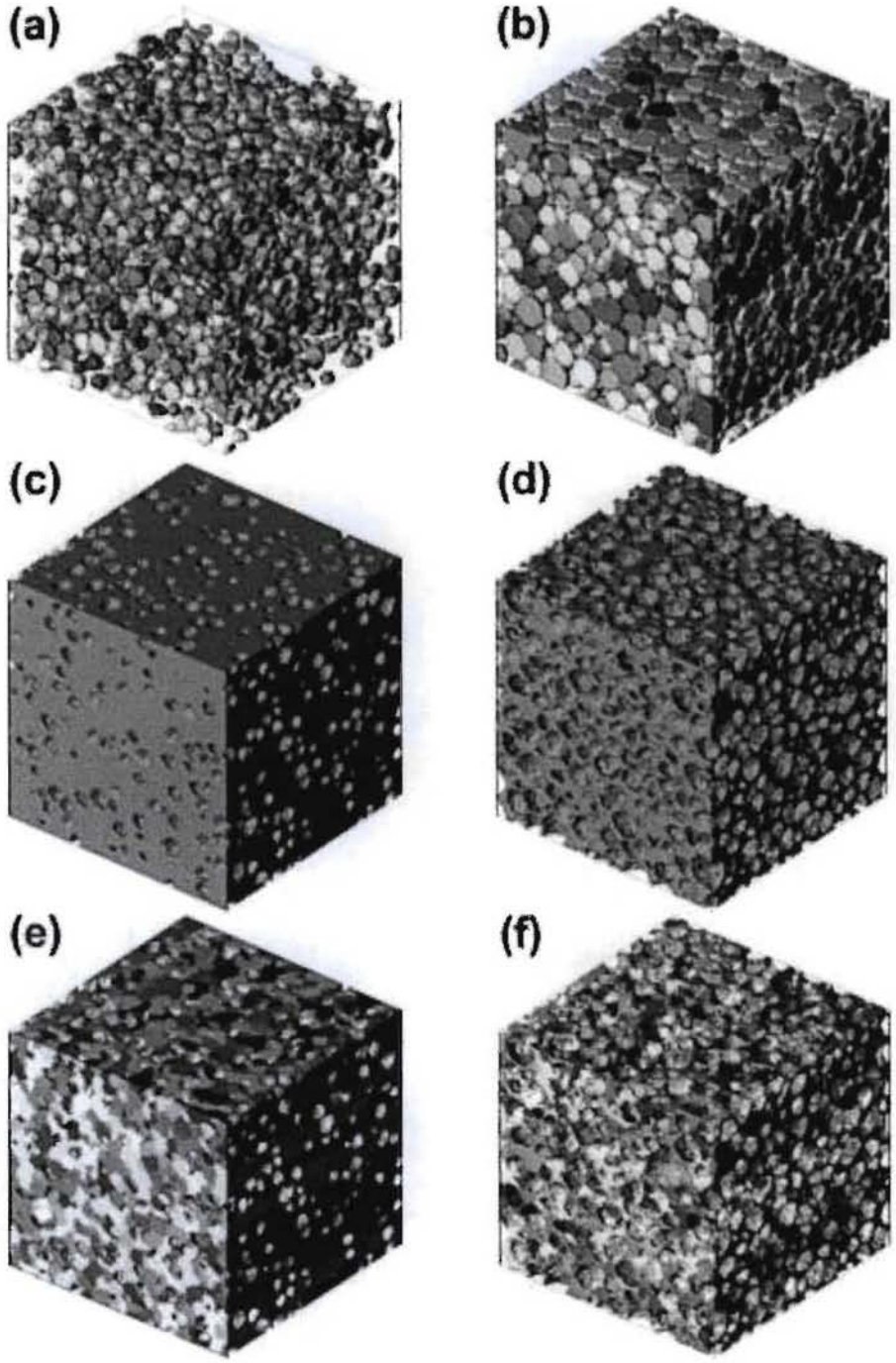

Fig. 1. (a) Particles from the coarsening simulation with volume fraction of ~ 0.2; (b) volume fraction of ~ 0.6 and the corresponding morphologies of the single crystal matrix, (c) and (d); and polycrystal matrix, (e) and (f). The particles and matrix grains are gray-scaled according to an arbitrary numbering scheme; the banding in color is only an artifact of the spatially progressive numbering.

polycrystalline matrix ((e) and (f)), for the particle volume fractions of ~ 0.2 and ~ 0.6. It is evident that the matrix has a percolating morphology due to the complete wetting condition imposed during coarsening simulation. Note also that, as the particle volume fraction increases, the grain shape in the matrix changes from a nearly equiaxed shape (Fig.1(e)) to an elongated one with branches between particles (Fig.1(f)).

2.2. Microstructural parameters

2.2.1. Volume fraction of particles (V_p)

While the composition of composite materials is typically expressed in the literature in weight-percent, for numerical simulations it is more directly expressed in terms of volume fraction. Also, the volume fraction of each phase is considered to be one of the crucial factors for determining equilibrium shapes and mechanical properties of sintered materials (German, 1998; Kim, 2004; Ratke and Voorhees, 2002). The volume fraction of particles, V_p, in the digital composite microstructure is defined as

$$V_p = N_p / N_{total} \quad , \tag{1}$$

where N_p and N_{total} are the number of voxels of particles and the total number of voxels in the simulation domain.

2.2.2. Contiguity of particles (C_p)

If the volume fraction of particles during the coarsening process is high, it is inevitable that particles in the system will contact each other, causing their shapes to be distorted from spheres (Lee et al., 2007; Park et al., 1989; Rowenhorst et al., 2006). Suppose we have two systems with the same number of particles and a similar particle size distribution, but with different volume fractions of particles. Then, it is intuitively reasonable to predict that the system with a higher volume fraction of particles has a greater chance that the particles are in contact with each other. Therefore, as the volume fraction of particles increases, we can expect that particle morphologies change both locally and globally such that the particles tend to form flat facets at the boundary regions and that they tend to develop a percolating skeletal structure within the system. Since morphological change of composite materials can strongly affect their properties, the degree of contact between particles in composite materials is an important microstructural parameter in predicting their properties.

In fact, the contiguity of particles in liquid phase sintered materials has been well recognized as an important factor influencing the properties of materials such as hardness, fracture toughness and strength in tungsten carbides (WC) in cobalt (Co) binder (Kim, 2004), thermal and electrical conductivity (Jernot and Chermant, 1982; Matsushita et al., 1977), and ductility (Churn and German, 1984) of liquid phase sintered materials. In particular, observation of the fracture surfaces of tungsten heavy alloys (W-Ni-Fe) revealed that the direct contact regions between tungsten particles were weaker than the other interphase bonding regions and, hence, at low strain-rate, cracks propagated along the contacting regions between tungsten particles (Churn and German, 1984).

The degree of contact between particles in composite materials can be measured by defining the contiguity of particles. The contiguity of particles, C_p, is defined as the ratio of the boundary area between particles, $A_{boundary}$, to the total surface area of the particles, $A_{surface}$ (German, 1985; Gurland, 1966; Kim, 2004). Then, the contiguity of

particles is defined as the average fraction of particle/particle boundary area per particle in the system with values ranging from 0 to 1.

$$C_p = 2A_{boundary} / A_{surface} . \quad (2)$$

In a simulated two-phase, composite microstructure, the contiguity of particles can be calculated as

$$C_p = N_{boundary} / N_{surface} , \quad (3)$$

where $N_{boundary}$ is the number of voxels at a particle/particle interface and $N_{surface}$ is the total number of surface voxels for all particles.

3. Property simulation method

The FFT-based formulation for viscoplastic polycrystals used in this work for property simulation is conceived for periodic unit cells, provides an "exact" solution (within the limitation imposed by the unavoidable discretization of the problem) of the governing equations. The viscoplastic FFT-based formulation consists in finding a strain-rate field, associated with a kinematically-admissible velocity field, which minimizes the average work-rate, under the compatibility and equilibrium constraints. The method relies on the fact that the local mechanical response of a periodic heterogeneous medium can be calculated as a convolution integral between the Green function of a linear reference homogeneous medium and a polarization (heterogeneity) field. Since convolution integrals reduce to a simple product in Fourier space, the FFT algorithm can be used to transform the Green function and the polarization field into Fourier space and, in turn, to get the mechanical fields by anti-transforming the product of this two quantities back to real space. Given that the actual polarization depends precisely on the a priori unknown mechanical fields, an iterative scheme should be implemented to obtain, upon convergence, a compatible strain-rate field and an equilibrated stress field. The FFT-based formulation has been thoroughly presented several times elsewhere (Lebensohn, 2001; Lebensohn et al., 2008; Lebensohn et al., 2009; Michel et al., 2000; Moulinec and Suquet, 1994; Moulinec and Suquet, 1998), and, in particular, the specialization to viscoplastic polycrystals can be found in Lebensohn and coworkers' works (2001, 2008, 2009). Therefore, in what follows we are giving just some key expressions of the method. The interest reader is referred to previous works, for further details.

The periodic unit cell representing the two-phase polycrystalline composite is discretized by means of a regular grid $\{\mathbf{x}^d\}$, which in turn determines a corresponding grid of the same dimensions in Fourier space $\{\xi^d\}$. An average strain-rate $\dot{E}_{ij}$ is imposed to the unit cell and the response to this mechanical solicitation, in terms of stress and strain-rate fields, has to be determined. The local constitutive equation that relates the deviatoric stress $\sigma'_{ij}(\mathbf{x})$ and the strain-rate $\dot{\varepsilon}_{ij}(\mathbf{x}) = \frac{1}{2}\left(v_{i,j}(\mathbf{x}) + v_{j,i}(\mathbf{x})\right)$ ($v_i(\mathbf{x})$: velocity field) at any given point $\mathbf{x}$ of the two-phase polycrystalline composite is assumed to be given by the crystal plasticity rate-sensitivity equation:

$$\dot{\varepsilon}_{ij}(\mathbf{x}) = \dot{\gamma}_0 \sum_{s=1}^{N_s} m_{ij}^s(\mathbf{x}) \left(\frac{\left| m^s(\mathbf{x}) : \sigma'(\mathbf{x}) \right|}{\tau^s(\mathbf{x})} \right)^n \operatorname{sgn}\left(m^s(\mathbf{x}) : \sigma'(\mathbf{x}) \right) \quad (4)$$

where m_{ij}^s and τ^s are, respectively, the Schmid tensor and the threshold stress of slip system (s); n is the rate-sensitivity exponent, $\dot{\gamma}_o$ is reference shear-rate and N_s the number of slip systems potentially active in the single crystal. The parameters τ^s, n and N_s depend on the phase to which the material point belongs, and m_{ij}^s also depends on the particular crystallographic orientation associated to that point.

With $p(\mathbf{x})$ being the hydrostatic pressure field, the Cauchy stress field can be written as:

$$\sigma_{ij}(\mathbf{x}) = L^o_{ijkl}\dot{\varepsilon}_{kl}(\mathbf{x}) + \varphi_{ij}(\mathbf{x}) - p(\mathbf{x})\delta_{ij} \tag{5}$$

where the polarization field $\varphi_{ij}(\mathbf{x})$ given by:

$$\varphi_{ij}(\mathbf{x}) = \sigma'_{ij}(\mathbf{x}) - L^o_{ijkl}\dot{\varepsilon}_{kl}(\mathbf{x}) \tag{6}$$

where L^o is the stiffness of a linear reference medium. Combining Eq. (6) with the equilibrium and the incompressibity conditions gives:

$$\begin{cases} L^o_{ijkl}v_{k,lj}(\mathbf{x}) + \varphi_{ij,j}(\mathbf{x}) - p_{,i}(\mathbf{x}) = 0 \\ v_{k,k}(\mathbf{x}) = 0 \end{cases} \tag{7}$$

The system of differential equations (7), with periodic boundary conditions across the unit cell boundary, can be solved by means of the Green function method. If G_{km} is the periodic Green functions associated with the velocity field, the solution of system (7) for this field is a convolution integral between the corresponding Green function and the polarization field. Taking derivatives and symmetrizing, the strain-rate field is given by:

$$\dot{\varepsilon}_{ij}(\mathbf{x}) = \dot{E}_{ij} + FT^{-1}\left\{\hat{\Gamma}^{sym}_{ijkl}(\xi)\hat{\varphi}_{kl}(\xi)\right\}(\mathbf{x}) \tag{8}$$

where $\Gamma^{sym}_{ijkl} = sym\left(G_{ik,jl}\right)$ and FT^{-1} indicates inverse Fourier transform. The tensors $\hat{G}_{ij}(\xi)$ and $\hat{\Gamma}^{sym}_{ijkl}(\xi)$ are only functions of L^o and can be readily obtained for every point belonging to $\{\xi^{\mathbf{d}}\}$ (for details, see Lebensohn et al., 2008). Having current guess values of the strain-rate field in the regular grid $\{\mathbf{x}^{\mathbf{d}}\}$ and computing the corresponding stress field from the local constitutive relation (Eq. 4) allow us to obtain a guess for the polarization field in direct space $\varphi_{ij}\left(\mathbf{x}^{\mathbf{d}}\right)$ (Eq. 6), from which, by application of FFT, $\hat{\varphi}_{ij}\left(\xi^{\mathbf{d}}\right)$ can be readily calculated. An improved guess for the strain-rate field in $\{\mathbf{x}^{\mathbf{d}}\}$ can be then obtained with Eq. (8), etc. The actual iterative procedure used in the viscoplastic present case requires the application augmented Lagrangians algorithm (Michel et al., 2000) that guarantees that the converged stress and strain-rate fields fulfill equilibrium and compatibility, respectively (see works by Lebensohn et al. (2008) and Michel et al. (2000) for details).

At this point, it is necessary to mention some additional assumptions made for the property simulations that follow. As previously mentioned, the input microstructures from coarsening simulations have voxelized data with periodic boundary conditions. So, we can use directly the resulting digital composite microstructures as input for the

property simulation. In all subsequent property simulations, stress and strain rate fields are calculated for uniaxial tension. The following conditions are consistently imposed: 1) the number of Fourier grid points coincide with the number of voxels of the input microstructures; 2) each particle is a single BCC crystal with a randomly chosen orientation, so that the ensemble of the BCC particles has a nearly random texture; 3) the matrix is considered to be a solid consisting of either a single FCC crystal (case of microstructures shown in Figs. 1(c) and 1(d)) with an orientation (in Bunge angles) given by (ϕ_1, Φ, ϕ_2) = (0°, 0°, 0°) (known as the "cube" orientation), or an FCC polycrystal with a random texture (case of Figs. 1(e) and 1(f)); 4) the threshold resolved shear stress (i.e. τ^s in Eq. 4) of the BCC phase associated with the 12 {110}<111> and the 12 {112}<111> potentially active slip systems is set to be 1.0 in arbitrary units (a.u.); and 5) the yield stress that BCC particle phase would have if it would fill the entire unit cell is set to be twice the yield stress of the FCC matrix phase (amounting to introduce a contrast factor $X=2$ between the phases). Under this condition, the threshold stress of the 12 {111}<110> slip systems in FCC crystal is found to be 0.554 in a.u. This threshold stress is also used when the matrix is polycrystalline in order to assess the effect of polycrystallinity of matrix on the overall mechanical response of the material.

As an illustration of the property simulation methodology, consider a simulation on a 128×128×128 system from the coarsening simulation with 128×128×128 Fourier grid points. One cross-section of the microstructure and the corresponding stress and strain rate field sections are shown in Fig. 2. Note that the highest strain rate values are found in the matrix phase, following 45° paths, which are soft shear planes in the FCC crystal with the cube orientation. Hot spots in strain rate are located either along boundaries or at interstices between particles. In general, for the assumed phase contrast, the stress is concentrated in the particle phase while the matrix phase experiences heavy deformations. In the following sections, we will show that the stress and strain rate distributions are strongly affected by the microstructural parameters.

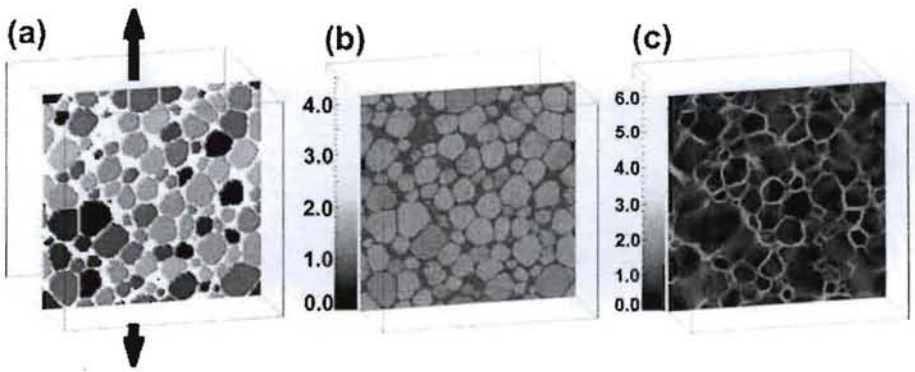

Fig. 2. Cross-sections through a representative 3D simulation showing (a) the input microstructure with particles gray-scaled arbitrarily (and the matrix omitted); (b) stress field, and (c) strain rate field (in a.u.). The arrows indicate the direction of applied uniaxial tension. Note that the stress and strain rate fields are inhomogeneous, both because of the imposition of the contrast factor between two phases (factor of two in flow stress) and the local heterogeneity of the microstructure.

4. Results

4.1. Effect of Morphology of Phases on Stress and Strain Rate Fields

4.1.1. Coarsened vs. "Disordered" Microstructures

In order to examine the effect of the morphology of the microstructure on the distributions of stress and strain rate under uniaxial tension, two different microstructures were prepared as shown in Fig. 3. Fig. 3(a) shows a microstructure from the Monte Carlo coarsening simulation with a prescribed solid volume fraction of ~ 0.6 (the exact volume fraction of solid voxels after the cleaning process was 0.5982) while Fig. 3(b) shows a "disordered" polycrystal (a single phase polycrystal obtained from the Monte Carlo isotropic grain growth simulation), within which grains are randomly selected (hence, the designation as "disordered") and assigned to be the matrix phase (soft FCC crystal with the "cube" orientation) so that the volume fraction of the remaining hard BCC grains is approximately 0.6 (the exact volume fraction of the BCC grains left is 0.5988). Also, in order to minimize the effect of the variation of other microstructural features on the simulation results, the microstructures were selected such that the numbers of hard BCC particles in both microstructures (hence, the average volume of those particles) were similar (see Table 1) and they were assigned the same set of random orientations. In both Figs. 3(a) and 3(b), the matrix was omitted for a better visualization of the difference in overall morphologies of two microstructures. Note that the "disordered" polycrystalline microstructure, Fig. 3(b), has a higher contiguity of particles, due to the flat boundaries between grains, than the coarsened microstructure, Fig. 3(a), while the matrix phase in the coarsened microstructure is fully percolating throughout the system (see also Figs. 1(c) and 1(d)) as opposed to the "disordered" microstructure where matrix phase actually forms isolated second phase regions and the particle phase is almost fully percolating as clusters.

After simulations were performed on both microstructures shown in Fig. 3, the average macroscopic stress $\bar{\sigma}^{VM}_{macro}$ of the composite microstructure and the relative activity χ in both particle phase and matrix phase were calculated using the following equations.

$$\bar{\sigma}^{VM}_{macro} = \left(\sum_{i=1}^{N} \sigma_i^{VM} \right) / N \tag{9}$$

$$\chi_{particle} = \left(\sum_{j=1}^{P} \dot{\varepsilon}_j^{VM} \right) / \left(\sum_{i=1}^{N} \dot{\varepsilon}_i^{VM} \right) \tag{10}$$

$$\chi_{matrix} = \left(\sum_{k=1}^{N-P} \dot{\varepsilon}_k^{VM} \right) / \left(\sum_{i=1}^{N} \dot{\varepsilon}_i^{VM} \right) \tag{11}$$

where N is the total number of the Fourier grid points, P is the number of Fourier grid points assigned to the particle phase, σ_i^{VM} is the von Mises stress at the ith Fourier point and $\dot{\varepsilon}^{VM}$ is the von Mises strain rate at the corresponding Fourier point. Since the total number of the voxels in either microstructure is equal to the total number of Fourier points N, then P and $(N\text{-}P)$ are proportional to the volumes of the particles and the matrix, respectively. The relative activity χ can be interpreted as the ratio of the strain rate carried by each phase, relative to the total strain rate.

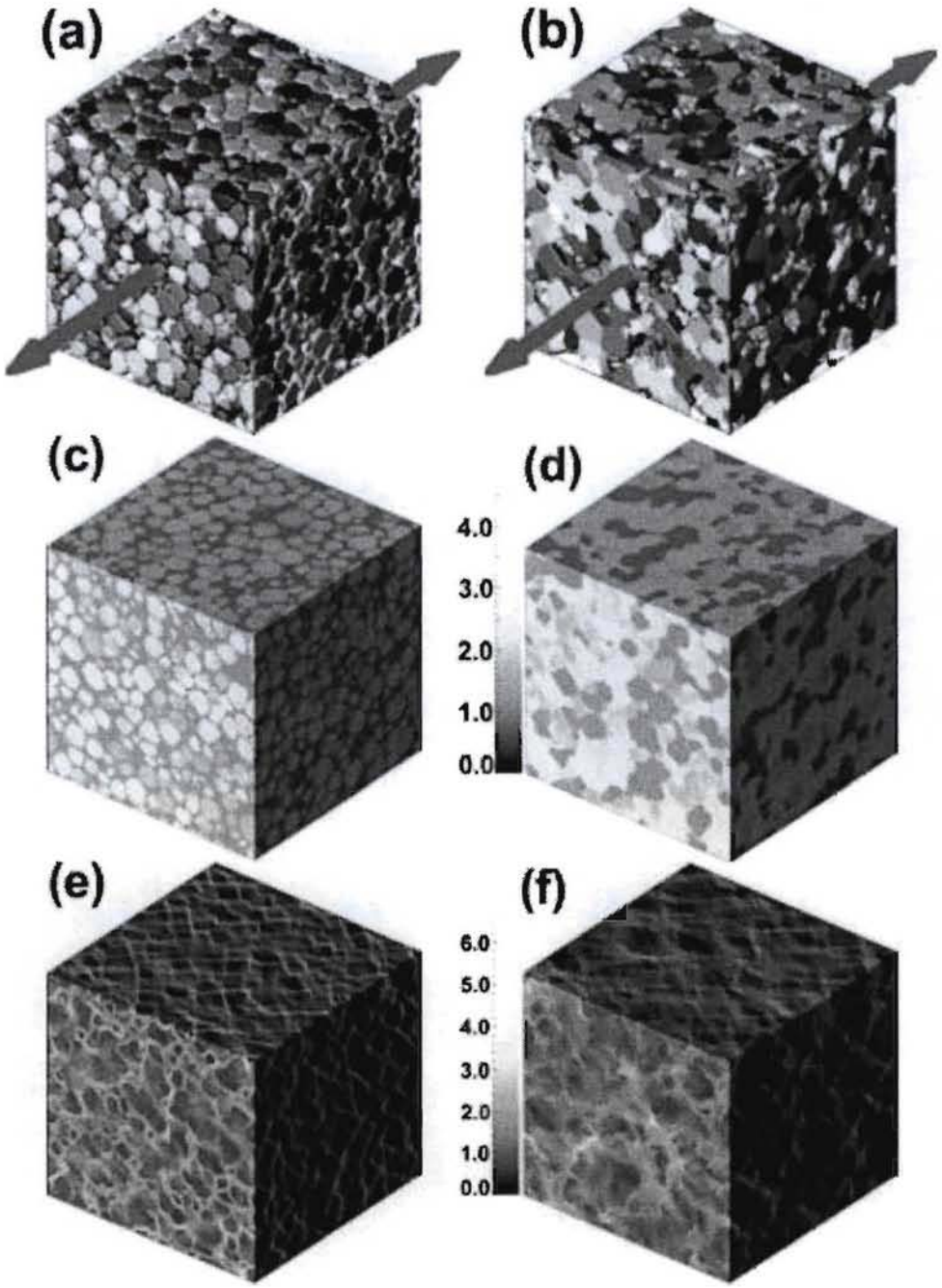

Fig. 3. Two contrasting microstructures used for instantiation of the simulations: (a) a microstructure from the coarsening simulation with particle volume fraction of ~ 0.6; (b) a modified single-phase polycrystal ("disordered" microstructure) wherein about 40 vol% of grains have the properties of the matrix phase. Figs. (c) and (d) are the corresponding stress fields, and (e) and (f) are the strain rate fields from the simulation of uniaxial tension in the coarsened and modified polycrystal microstructures, respectively. Note the drastic difference in morphologies of two microstructures and its effect on stress and strain rate fields. The arrows indicate the direction of applied uniaxial tension.

While the difference in the macroscopic average stresses for the two microstructures is small, i.e. $\overline{\sigma}_{macro}$ of the "disordered" polycrystalline microstructure is larger by about 9% compared to that of the coarsened microstructure (1.893 for the coarsened microstructure and 2.061 for the "disordered" microstructure), the relative strain rate activities of the two phases in the different microstructures are quite different. While χ_{matrix} of the "disordered" microstructure is 0.433, χ_{matrix} of the coarsened microstructure is 0.595 (37% increase), which means that the matrix phase in the coarsened microstructure takes up a larger fraction of the total strain rate in the system. This is due to the particular morphology of the coarsened microstructure. As mentioned before, the matrix phase in the coarsened microstructure is percolating throughout the system and hence develops thin channels between the particles (fully-wetting condition). The results from these simulations are also summarized in Table 1.

4.1.2. Variation in Relative Activity with Particle Volume Fraction

Let us now examine how the mechanical responses of the above two microstructures vary with the volume fraction of particles. For that, we generated two types of microstructures (coarsened and "disordered") with volume fraction of particles in the range of ~0.6, ~0.7 and ~0.8. For each volume fraction, the number (hence, the average volume) of particles in both types of microstructures is similar (see Table 2) and the particles are assigned with the same set of random orientations. Like before, the soft FCC matrix has the single "cube" orientation for both types. Fig. 4 shows the variation of the relative activity χ of each phase as a function of volume fraction of particles. Thick and thin solid lines are the ideal relative activities of particle phase and matrix phase, respectively, if the material is assumed to have phase contrast X=1 (i.e., if, in average, the two phases have no distinction in terms of mechanical response). Also, one can construct the same ideal lines for each phase when X=2 (thick and thin dashed lines), assuming that the matrix phase takes exactly twice the strain rate than the particles. For both microstructures, the matrix phase takes up more strain rate than the particle phase per unit volume while the matrix in the coarsened microstructure experiences a larger concentration of strain rate than in the "disordered" microstructure. Note that the relative activity of the matrix phase in the coarsened microstructure (solid triangles) tends to exceeds the estimate for X=2 (thin dashed line) as the particle volume fraction decreases while that in the "disordered" microstructure (open triangles) experiences much smaller strain rates, close the ideal case for X=1 (thin solid line). Again, due to the fully-wetting condition during the coarsening simulation, the percolating matrix in the coarsened microstructure develops thin channels between the particles, which makes it accommodate more deformation than the localized matrix phase in the "disordered" microstructure. As expected, in all cases, the relative activity of each phase converges to one point as the volume fraction of particles approaches unity.

4.2. Microstructures from the Monte Carlo Potts Coarsening Model

This section analyzes the stress and strain rate fields developed in the microstructures obtained from the Monte Carlo coarsening simulations when uniaxial tension is applied. First, the effect of the volume fraction of particles on the distributions of the stress and strain rate is examined. Second, the effect of other microstructural

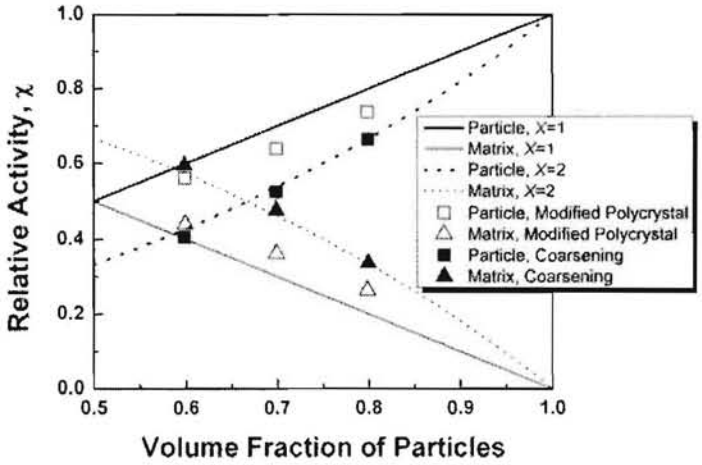

Fig. 4. Comparison of the variation of the relative activity of each phase as a function of volume fraction of particles in both coarsened microstructure and modified polycrystal. Note a significant offset in the relative activity for each phase between the "disordered" and the coarsened microstructures. Also, the results are compared to two ideal cases when the contrast factor $X = 1$ and 2 (solid and dashed lines, respectively). Note the drastic effect of morphology of the matrix phase on the relative activity of each phase such that the matrix phase in the coarsened microstructure (solid triangles) takes up more strain than the ideal case for X=2 (thin dashed line) as the particle volume fraction decreases while that in the "disordered" microstructure (open triangles) experiences much smaller deformation close the ideal case for X=1 (thick solid line).

parameters on the mechanical response is explored by comparing the results from property simulations using input microstructures with different number and contiguities of particles, while the volume fraction of particles remains fixed. Third, the evolution of the stress distribution in the hard BCC particles is examined as a function of the particle volume fraction. Finally, the effect of the polycrystallinity of matrix on the stress and strain rate distributions is studied by comparing the results with those from microstructures where the matrix was a single crystal with the "cube" orientation.

In the following sections, the average stress and strain rate in both phases and in the entire composite microstructure are calculated using the following equations.

$$\bar{\sigma}^{VM}_{macro} = \left(\sum_{i=1}^{N} \sigma_i^{VM}\right)/N \;;\; \dot{\bar{\varepsilon}}^{VM}_{macro} = \left(\sum_{i=1}^{N} \dot{\varepsilon}^{VM}_{macro}\right)/N \qquad (12)$$

$$\bar{\sigma}^{VM}_{particle} = \left(\sum_{j=1}^{P} \sigma_j^{VM}\right)/P \;;\; \dot{\bar{\varepsilon}}^{VM}_{particle} = \left(\sum_{j=1}^{P} \dot{\varepsilon}_j^{VM}\right)/P \qquad (13)$$

$$\bar{\sigma}^{VM}_{matrix} = \left(\sum_{k=1}^{N-P} \sigma_k^{VM}\right)/(N-P) \;;\; \dot{\bar{\varepsilon}}^{VM}_{matrix} = \left(\sum_{k=1}^{N-P} \dot{\varepsilon}_k^{VM}\right)/(N-P) \qquad (14)$$

4.2.1. Effect of Volume Fraction of Particles on Stress and Strain Rate Fields in Coarsened Microstructures

In this section, we consider the effect of varying the volume fraction while holding all other variables constant. All microstructures were generated by simulation of

coarsening as described in section 2.1 (for example, Fig. 1 shows two microstructures with different volume fractions of particles). The particle volume fractions were varied between 0.2 and 0.8. For each volume fraction, four to six microstructures were selected from the same coarsening simulation at different times in order to evaluate the variation with average particle size, number of particles and contiguity of particles, while holding volume fraction constant. For each selected microstructure, three different random orientation sets were used for property simulation and the results were averaged. The results of this section correspond to a "cube"-oriented single crystal matrix phase.

Fig. 5 shows the average stress and strain rate plotted against the volume fraction of particles (for a simulation domain size of 128x128x128). Also shown are dashed lines that represent the linear fits to the data for both phases. The values at particle volume fractions of 1.0 and 0.0 (black solid dots) were obtained from simulations on a BCC polycrystal with a random texture and a FCC single crystal with the "cube" orientation, respectively, with the other simulation parameters unchanged. Since we chose four to six different microstructures for each volume category, the spread of the data for each phase corresponding to a specific volume fraction can be understood as the variation in the average properties due to the different number of particles, contiguity of particles and etc. Note that the average properties for both phases exhibit an almost linear dependence on the particle volume fraction with small variance over the most of the range, except for volume fractions near 0.0 or 1.0, suggesting that different instantiations of the coarsened microstructures lead to negligible variation in average stress and strain rate. Also, note that the average stress of the overall composite is within the bounds predicted from the simple rules of mixtures, $\sigma_{mixture}=\sigma_p V_p+\sigma_m V_m$ and $\sigma_{mixture}=\sigma_p\sigma_m/(\sigma_p V_m+\sigma_m V_p)$. σ_p and σ_m are the average stresses for the particle phase and the matrix phase obtained from

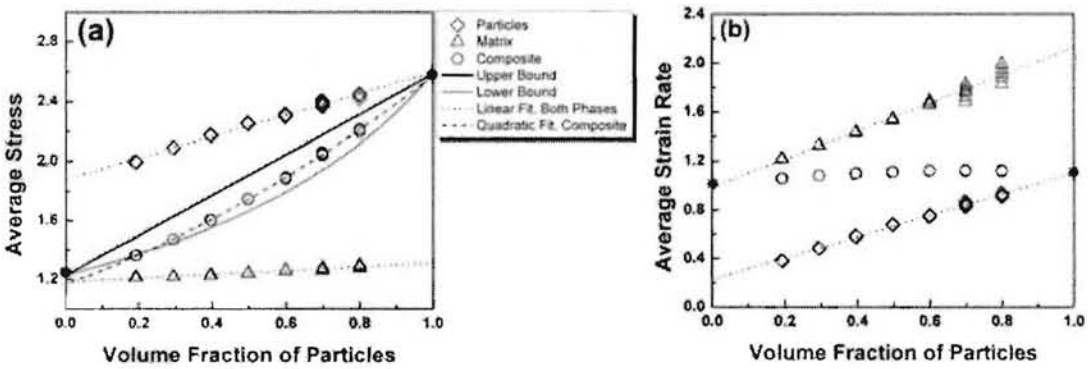

Fig. 5. (a) Average stress and (b) average strain rate as a function of volume fraction for each phase and for overall microstructure computed for uniaxial tension. The average strain rate is imposed as a boundary condition so the variation in the two phases with volume fraction is as expected from partitioning of the strain rate between the two phases. The values at particle volume fractions of 1.0 and 0.0 (black solid dots) are obtained from simulations on a polycrystal with BCC grains with a random texture and a FCC single crystal with the cube orientation, respectively. Note that different instantiations at each volume fraction lead to only minor variations in the outcome, which is most evident at high fractions in the matrix phase. Also, note that average stress in composite is within the bounds predicted by the simple rules of mixtures.

simulations on a random BCC polycrystal and a "cube"-oriented FCC single crystal as explained before (σ_p=2.587 and σ_m=1.229, respectively, as black solid dots in the figure). $\sigma_{mixture}$ is the effective stress of the overall microstructure, and V_p and V_m are the volume fraction of the particles and the matrix such that V_p+V_m=1.0.

4.2.2. Effect of Morphological Change with Constant Particle Volume Fraction on Stress and Strain Rate Fields in Coarsened Microstructures

During a coarsening simulation, the microstructure evolves such that the number of particles decreases, the average size of particles increases and the contiguity of particles decreases. The morphological changes of these individual microstructural features occurring during coarsening are inevitable and are dependent on each other due to the mass conservation condition imposed in the coarsening simulation (Lee et al., 2007). Having said that, it is of interest to examine the effect of morphological changes in the microstructures with the same particle volume fraction from a single coarsening simulation run. In fact, one piece of evidence for such effect can be qualitatively observed from Fig. 5, where there is a spread in the stress and strain rate for each phase at each particle volume fraction (especially, 0.7 and 0.8). This motivates a more detailed examination of these morphological changes in order to quantify the sensitivity of the mechanical response to microstructural variations other than volume fraction. As the first step towards this goal, two different microstructures (128×128×128) from a single coarsening simulation, both with a particle volume fraction of ~0.7, were chosen such that one of them has high contiguity of particles and the other a low one. The two microstructures are shown in Fig. 6.

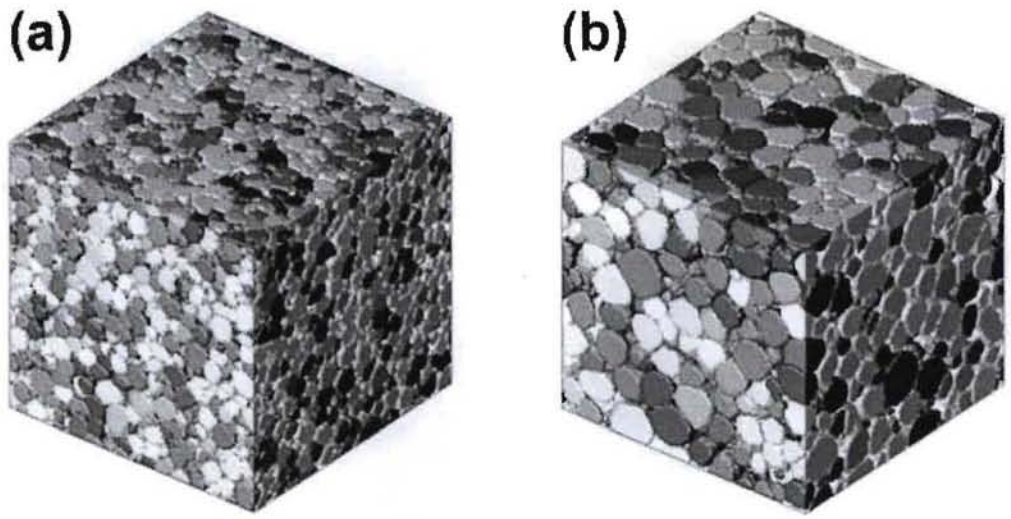

Fig. 6. Microstructures from a single coarsening simulation run with the particle volume fraction of about 0.7 having (a) high contiguity and (b) low contiguity of particles.

Note that the microstructure with high contiguity (0.5960, Fig. 6(a)) has a larger number of particles and smaller average particle size than the one with low contiguity

(0.2443, Fig. 6(b)). The macroscopic responses of the two microstructures are summarized in Table 3. Note that the relative activity of the matrix phase in the microstructure with low contiguity increases slightly (~7.0%), which results from the more percolating nature of the matrix in the microstructure than the one with high particle contiguity, such that particles carry more of the load. As is evident from Fig. 5, however, the macroscopic average stress and average strain rate in both microstructures are very similar, which implies that the macroscopic average mechanical response is most strongly dependent on the volume fraction of each phase in the microstructure, compared to the other microstructural parameters.

However, this does not guarantee that local responses of the microstructures to the applied external force are the same. To extract local information on stress and strain rate of each phase in the microstructure, one needs to examine the standard deviations of the local stress and strain rate for each phase. Fig. 7 shows the cross sections of the two microstructures with high particle contiguity, Fig. 7(a), and low particle contiguity, Fig. 7(b), and the corresponding stress fields, Figs. 7(c) and 7(d). The results of the stress analysis are summarized in Table 4. As previously mentioned, the macroscopic average stresses of the two microstructures are nearly the same. Note that the average stress is insensitive to differences in contiguity of particles. In contrast, the standard deviation in stress of the matrix phase in the microstructure with low particle contiguity is much larger, by ~24%, compared to the one with high particle contiguity, which suggests that the stress field in the matrix for the low contiguity case has a wider distribution of stress values than the high contiguity case. Nevertheless, the change in the shape of the stress distribution in the matrix is negligible because the change in the standard deviation in stress in the matrix phase with the change in particle contiguity is small relative to the corresponding average stress.

The results of the strain rate field and its standard deviation for each phase in both microstructures are quite different from those for the stress analysis. The strain rate fields of the two microstructures are also presented in Figs. 7(e) and 7(f), and the results of the corresponding strain rate analysis are summarized in Table 5. The figures suggest, qualitatively, that there are more hot spots in strain rate in the low contiguity microstructure. While the average strain rate and its standard deviation for the particle phase are insensitive to changes in the contiguity between particles, the average strain rate for the matrix phase are by ~8.4% larger in the microstructure with low contiguity of particles. This tendency is especially obvious for the standard deviation of strain rate in the matrix phase in the low particle contiguity microstructure (37.0% increase).

This trend is reasonable because, as the contiguity of particles decreases during coarsening, more complete wetting of particles by the matrix phase occurs. In other words, coarsening results in a percolating network of well-developed thin matrix channels at particle/particle boundary regions, giving longer paths in space along which the matrix phase can stretch out, which results in a higher average strain rate in the matrix phase for the microstructure with the low particle contiguity and more hot spots in the matrix phase. However, some cold spots are still present locally in the microstructure, when compared to the matrix phase in the high contiguity microstructure, which exhibits a larger standard deviation in strain rate. These cold spots are where the matrix is isolated in space, and it is also evident from Fig. 3 and Table 1 that the isolated matrix grains in the modified polycrystal have lower relative activity than those in the coarsened

microstructure. Figs. 7(e) and 7(f) show this trend qualitatively in the maps of strain rate in the cross sections of the microstructure.

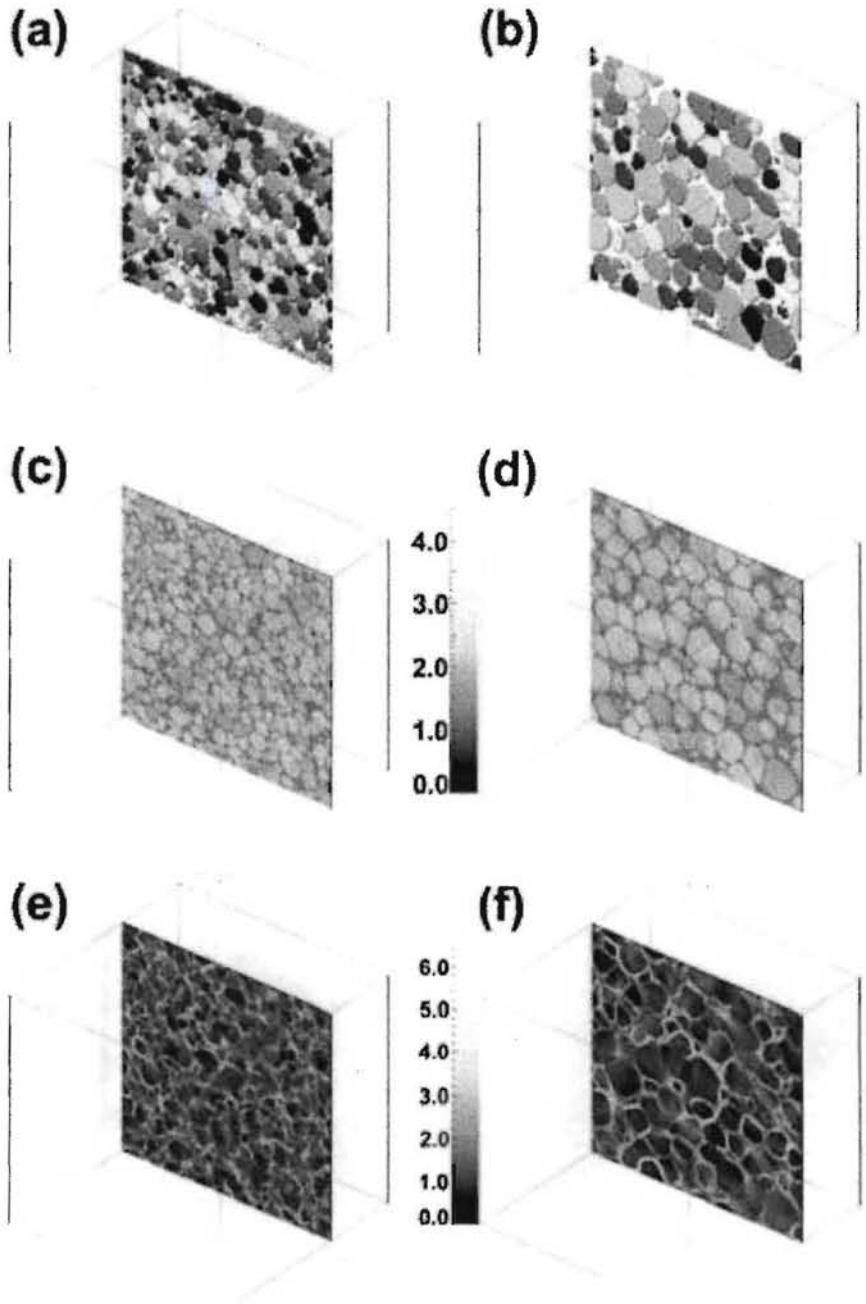

Fig. 7. Cross sections of microstructures having (a) high particle contiguity and (b) low particle contiguity in Fig. 6 under uniaxial tension and the corresponding stress fields ((c) and (d)), and strain rate fields ((e) and (f)).

In Fig. 8, the stress and strain rate distributions in both phases of the microstructures with different particle contiguities in Fig. 7 are presented: stress distribution in the particles, Fig. 8(a), stress distribution in the matrix, Fig. 8(b), strain rate distribution in the particles, Fig. 8(c), and strain rate distribution in the matrix, Fig. 8(d). At first glance, the distributions appear to be very similar between the high contiguity and low contiguity cases. Indeed, for the stress distributions, the average stress and its standard deviation in the two phases for both cases remain very similar as previously noted in Table 4. Even though the standard deviation in stress of the matrix phase increases significantly in percentage terms as the particle contiguity decreases, the difference is negligible when compared to its average value. Therefore, the stress is insensitive to variations in particle contiguity at both macroscopic scale and in terms of local behavior. However, the strain rate distributions in the two phases for both cases reveal something interesting. In particular, the matrix phase in the coarsened microstructure with low contiguity has a wider distribution of strain rate with a lower maximum peak than that with high contiguity, Fig. 8(d), whereas the increase in the corresponding average strain rate is relatively small (8.4%, Table 5). This is also evident in Table 5 as the drastic increase in the standard deviation of the strain rate in the matrix phase in the coarsened microstructure with low particle contiguity (37% increase from high to low contiguity). Fig. 9 shows the differences in the frequencies between the two coarsened microstructures (as number fractions) for stress and strain rate in the two phases. The frequency difference is calculated as $f_{high\_contiguity} - f_{low\_contiguity}$ for each bin. The stress distribution slightly shifts to the right for the particles with a higher contiguity, Fig. 8(a), while that of the corresponding the matrix phase slightly moves to smaller values, Fig. 8(b). This is reasonable because the particles with smaller average size will have higher particle contiguity and take up more stress for fixed particle volume fraction. Fig. 9 also shows that positive values of the frequency difference at larger stress values are found for the particles whereas the stress distribution of the matrix phase is narrower in the higher particle contiguity case. Also, note the negative values of the frequency difference at large strain rates in the matrix phase, which reveals the drastic increase in standard deviation of strain rate for the matrix phase in the microstructure with low particle contiguity.

To see the trend more clearly, the same property simulations were performed on the microstructures that were chosen from the same coarsening simulation run with particle volume fractions of ~0.6, ~0.7 and ~0.8. The input microstructures were chosen such that the corresponding contiguity of particles varies approximately from ~0.3 to ~0.6 for each volume category. In each phase for all volume categories, only a slight variation is observed in average stress and its standard deviation as a function of the particle contiguity as previously observed. However, the average strain rate and its standard deviation in matrix phase are found to be a strong function of the particle contiguity. The results from the property simulations for the particle volume fraction of ~0.8 are summarized in Fig. 10 as an example. Note that the standard deviation of strain rate in the matrix phase is very sensitive to the contiguity of particles and decreases linearly as the particle contiguity increases.

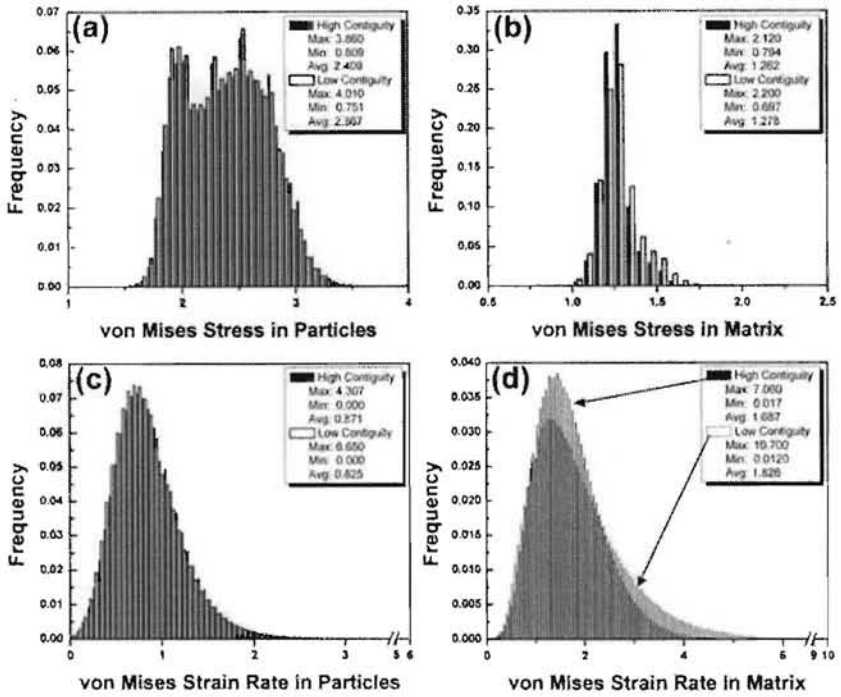

Fig. 8. Stress and strain rate distributions in both particle ((a) and (c)) and matrix ((b) and (d)) phases of the coarsened microstructures with high particle contiguity (solid bars) and with low particle contiguity (open bars) in Fig. 7. Note that strain rate distribution of the matrix phase in the coarsened microstructure with low particle contiguity has a wider shape, compared to high contiguity case.

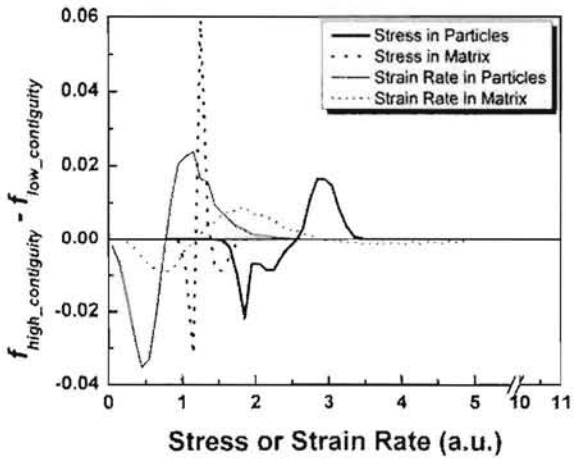

Fig. 9. Differences in the frequencies for stress and strain rate of the two phases in both coarsened microstructures with different particle contiguities are presented, defined as $f_{high\_contiguity} - f_{low\_contiguity}$ for each bin. Note the negative values of the frequency difference in strain rate of the matrix phase over the bins with large values, which highlights the substantial increase in standard deviation of strain rate for the matrix phase in the microstructure with low particle contiguity.

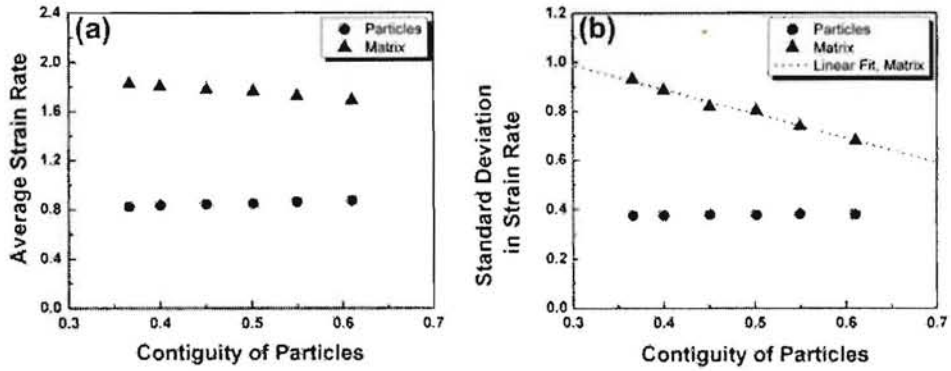

Fig. 10. Average strain rate and its standard deviation of both particles and matrix phase in the microstructures from coarsening simulation with particle volume fraction of ~ 0.8 as a function of contiguity of particles. Note that the standard deviation of strain rate decreases strongly in a linear fashion in the matrix with increasing particle contiguity.

4.2.3. Effect of Morphological Change on the Stress Distribution in Particles

In the previous section, we observed that the stress distribution of the particle phase in the composites under uniaxial tension is weakly dependent on contiguity. This interesting trend prompted an examination of the dependence of the stress distribution of the particles on their volume fraction. Fig. 11 shows the variation in the stress distribution of the hard BCC particle phase under uniaxial tension as a function of the particle volume fraction. Also, two more cases are considered and compared to the results from the composite microstructures: 1) FFT plasticity simulation on a polycrystal under uniaxial tension, having ~2,500 BCC grains with random texture, with several different viscoplasticity exponents n = 10, 20, 30 and 40; and 2) rate-insensitive Taylor factor calculation for 64^3 random orientations with BCC structure under uniaxial deformation. The latter calculation was performed with the commercial OIM^{TM} software package. For composite and BCC polycrystal cases, the microstructures with different particle volume fractions were chosen such that the number of particles was similar (~2,000) and, hence, the average size and the contiguity of particles increases as the particle volume fraction increases. Since a threshold resolved shear stress of 1.0 was used for all slip systems of BCC particles during simulations and assuming that the local Taylor factor in the BCC particles/grains from simulations is equal to local von Mises equivalent stress divided by the threshold stress, it is sensible to compare the stress distribution in the particles from simulations to that of Taylor factors of isolated BCC voxels in order to see the effect of the morphology of microstructures and the particle volume fraction on the stress distribution in the particles. The main result is a drastic but smooth transition of the stress distribution in the BCC particles with increasing particle volume fraction. At high volume fractions, the distribution tends to be towards that calculated for the BCC polycrystal. As the particle volume fraction increases, the average stress of the particles increases as noticed before, which results in the shift of the distribution curve to the right. At the microstructural scale, as the particle contiguity increases with increasing volume fraction, particles in soft orientations are no longer shielded by the softer matrix phase and load is transmitted to particles in harder

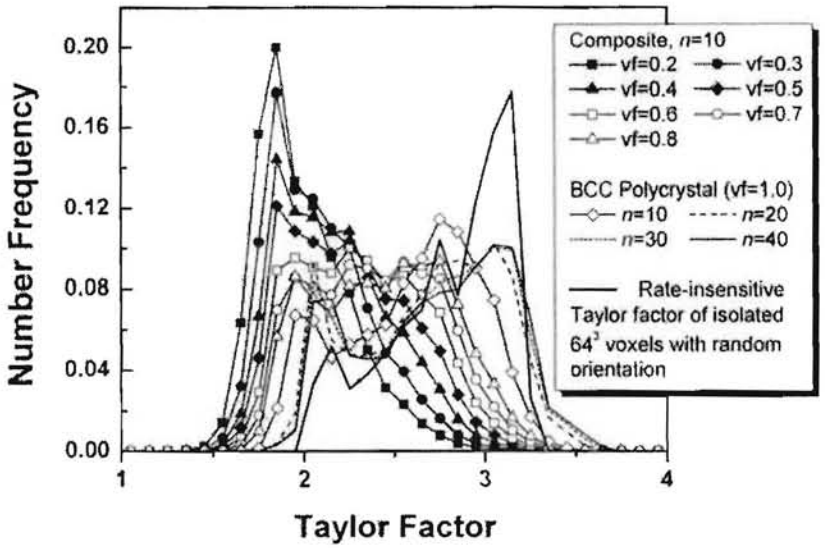

Fig. 11. Variation in the stress distribution of the hard BCC particles in the composite under uniaxial tension as a function of the particle volume fraction (vf), compared to two more cases; 1) FFT plasticity simulation on a polycrystal under uniaxial tension, having BCC grains with random texture, with varying the viscoplasticity exponent n = 10, 20, 30 and 40; and 2) Taylor factor calculation for 64^3 isolated voxels with BCC structure under uniaxial deformation, having random orientation. Note that the drastic but smooth transition of the stress distribution in the BCC particles with increasing particle volume fraction such that it agrees with the simulated stress distributions in the polycrystal with BCC grains as particle volume fraction approached unity. Also, note that, as n increases, the stress distribution tends to develop the maximum peak at high stress regime, which tends toward the Taylor factor distribution of isolated voxels.

orientations (i.e., at higher stresses). This provides a simple explanation for the changes in skewness from left to right as the particle volume fraction increases.

However, the distribution of Taylor factors from the 64^3 isolated BCC voxels is quite different from that of the FFT simulation on the same voxels in a 64×64×64 simulation domain. This is because of the effect from the neighbors on the stress and strain rate state for each voxel during the FFT simulation. Note that, as n increases, the results from the BCC polycrystal case evolve toward to match the distribution of Taylor factors when those 64^3 voxels are isolated with no neighboring interactions, such that the frequencies over the bins with both large and small stress values become higher while those over the intermediate bins get lower.

4.2.4. Single Crystal versus Polycrystal Matrix

Up to this point, the matrix phase has been treated as an FCC single crystal having a single orientation ("cube" orientation). In reality, however, the matrix phase solidifies after liquid phase sintering and is polycrystalline, as previously mentioned. In this section, we examine the effect of polycrystallinity of matrix on the stress and strain rate fields under uniaxial tension.

The change in the relative activity of each phase in the coarsened microstructures with a randomly oriented polycrystalline matrix is presented in Fig. 12, where the results are compared to those for the "cube"-oriented single crystal matrix. Since the "cube"

orientation is a soft orientation in uniaxial tension, it is reasonable that the relative activity in the polycrystal matrix is smaller than that in the single crystal matrix. Given the uniform strain boundary condition used for all property simulations, this decrease must be compensated by increase in the relative activity in particles. A decrease in the relative activity of the polycrystal matrix from that of a single crystal matrix is observed consistently across the range of particle volume fractions.

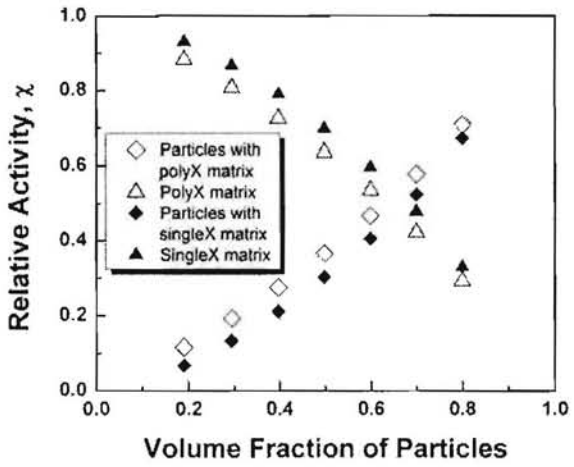

Fig. 12. The comparison of the relative activity of each phase as a function of volume fraction of particles in coarsened microstructures with either a single crystal matrix having the cube orientation or a polycrystal matrix having random orientation. Note a consistent decrease in the relative activity of the polycrystal matrix from that of the single crystal matrix.

Fig. 13 shows the stress and strain rate fields for both the single crystal matrix case, Figs. 13(a) and (c), and the polycrystal matrix case, Figs. 13(b) and (d), respectively, with particle volume fractions of ~0.6. The geometry of the microstructures is the same for the two cases and so the configuration of particles and matrix is the same. The only difference between two microstructures is that the one has a single crystal matrix whereas the other one has a polycrystalline matrix. Note that the gray-scaled color of the stress field is whiter for the polycrystalline matrix case, which corresponds to a higher macroscopic average stress. Note also that individual particles have different stress values for the two different matrices; this is also true for the matrix. The strain rate field for the polycrystalline matrix case, Fig. 13(d), has fewer hot spots and more diffuse gray-scaled color than the corresponding field in the single crystal matrix, Fig. 13(c). This suggests that the distribution of strain rate is more homogenous in the polycrystalline case.

Figs. 14 and 15 show the first and second moments for the stress and strain rate fields, comparing the polycrystal matrix case with the single crystal matrix case. For the composite as a whole, the average stress is substantially higher in the polycrystal matrix case whereas the standard deviation in stress is lower for all volume fractions except V_f= 0.2. The average strain rate is a boundary condition for the composite as a whole but its standard deviation is appreciably smaller in the polycrystal matrix compared to the single crystal matrix. Considering the matrix by itself, both the average stress and the standard

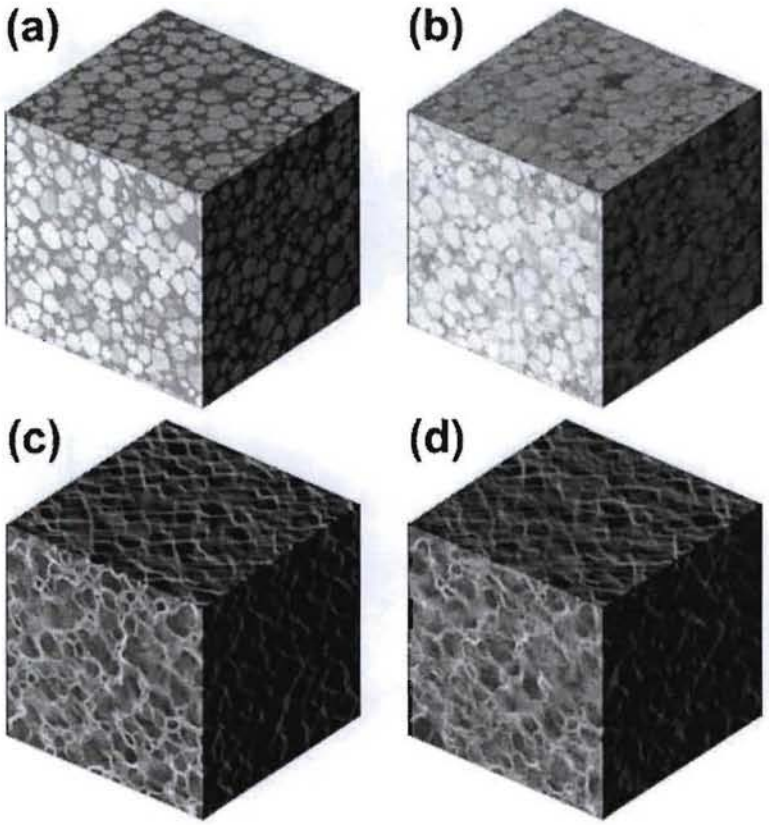

Fig. 13. Stress and strain rate fields in the microstructures with the particle volume fraction of ~ 0.6. (a) and (c) are stress and strain rated fields from the simulation on the microstructures with a single crystal matrix with the cube orientation, respectively, and (b) and (d) are stress and strain rated fields from the microstructures with a polycrystal matrix with random orientation, respectively. Note that more stress is transferred to the particles due to the polycrystallinity of the matrix phase, and that the more homogeneous distribution of strain rate in the microstructures is developed with a polycrystalline matrix than in that with the single crystal matrix.

deviation are appreciably higher in the polycrystal matrix. The average stress in the particles and its standard deviation are also higher in the particles, although the differences between the two matrices vanish at high particle volume fractions.

It is apparent that the heterogeneous polycrystalline matrix mor effectively transmits stress between particles, compared to single crystal case. Keeping with the relative activity analysis, Fig. 12, a polycrystalline matrix provides a harder, more heterogeneous matrix, such that it absorbs a smaller fraction of the imposed strain rate (smaller average strain rate with smaller standard deviation for the polycrystalline matrix). This is similar to the trend in the stress analysis in particles as a function of contiguity of particles (Table 1 for the "disordered" microstructure case and Table 4 for coarsening case), where the average stress in the particles increases as the contiguity of particles increases, albeit only by a small amount. Again, one can easily see that such particles that have different gray-scaled colors for stress between the two cases (Fig. 13).

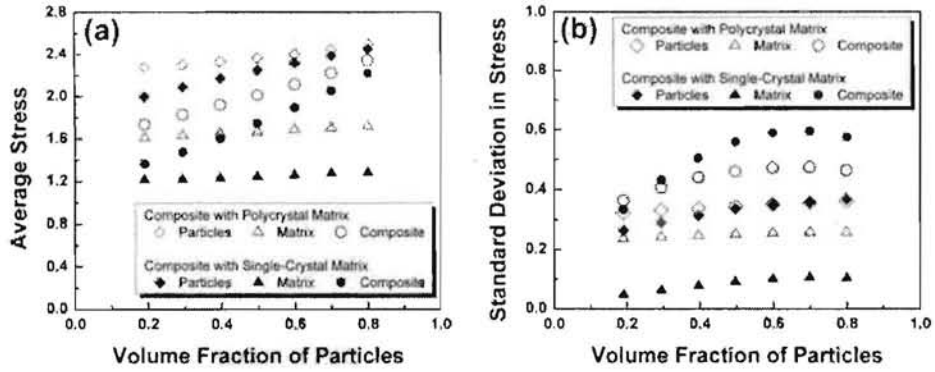

Fig. 14. (a) Average stress and (b) its standard deviation of both particles and matrix phase in the microstructures from coarsening simulation as a function of volume fraction of particles. The microstructures have the same set of particles and either a single crystal matrix with the cube orientation or a polycrystal matrix with random orientations.

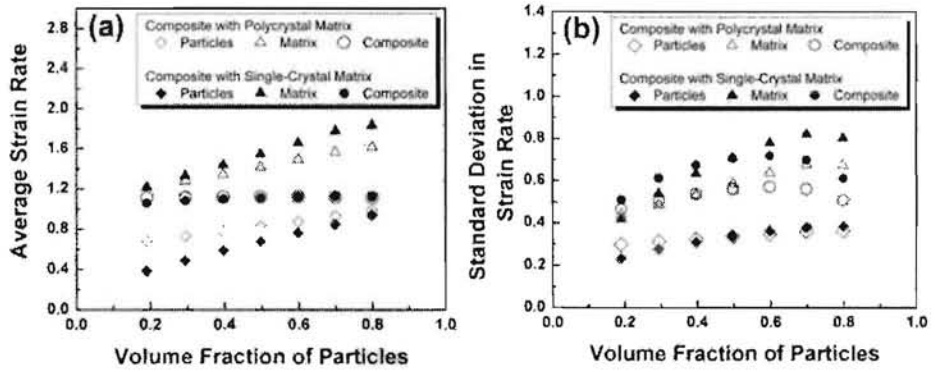

Fig. 15. (a) Average strain rate and (b) its standard deviation of both particles and matrix phase in the microstructures from coarsening simulation as a function of volume fraction of particles. The microstructures have the same set of particles and either a single crystal matrix with the cube orientation or a polycrystal matrix with random orientations.

5. Concluding Remarks

Simulations of the viscoplastic response under uniaxial tension using the Fast Fourier Transform (FFT) algorithm has been used to describe the fundamental mechanical behavior of metal-metal composite materials. The digital microstructures were generated using the Monte Carlo simulation of coarsening (Ostwald ripening) (Lee et al., 1007). Specifically, stress and strain rate fields were obtained in these composite materials with nearly equiaxed BCC particles in an FCC matrix. Digital composite materials were devised with a wide range of spatial distributions of particles and hence the different morphologies of the matrix phase.

Stress is mainly concentrated in the hard particle phase while the soft matrix phase takes up more of the strain rate because of the higher threshold resolved shear

stress imposed for the particles. The macroscopic response in terms of the average stress and average strain rate obeys the simple rule of mixtures. However, the variation in standard deviation in the strain rate is less simple, especially at high particle volume fractions, where the contiguity of particles has a noticeable effect on the mechanical response. This leads to the conclusion that the first moments of the stress and strain rate are relatively insensitive to the microstructure under these conditions whereas the second moments of the distributions are strongly dependent on the microstructure.

The particle volume fraction and the contiguity of particles appear to be the most important microstructural factors that affect the mechanical behavior, in that average stresses and strain rates, and their standard deviations for each phase and overall microstructure increase with both increasing particle volume fraction and with decreasing contiguity of particles (Chawla et al., 2004; Chawla and Chawla, 2006; Chawla et al., 2006b; Ganesh and Chawla, 2005; Kim, 2004;). At a fixed volume fraction, the mechanical response of composite materials, in terms of average stress and strain rate under uniaxial tension, is a strong function of the microstructure type. In particular, more strain rate is taken up by the percolating, wetting matrix phase in the coarsened microstructures than by locally isolated matrix grains in "disordered" polycrystalline microstructures. By contrast, the particles in the "disordered" microstructures sustain more stress than in the coarsened microstructure because of the higher particle contiguity in this type of microstructure.

As particle volume fraction approaches unity, the stress distribution in the BCC particles tends towards the simulated stress distributions expected in a BCC polycrystal. The average stress of the particles increases (shift of the distribution curve to the right) and particles start to lose the shielding from the softer matrix phase, which shifts the skewness of the stress distribution from left to right. However, even at the highest volume fractions, the distribution is noticeably different from the distribution of Taylor factors from the 64^3 isolated BCC voxels because of the effect from the neighbors on the stress and strain rate state for each voxel during the FFT simulation. As the viscoplasticity exponent, n, increases, the results from the FFT simulations on the BCC polycrystal tend towards the distribution of Taylor factors for the same set of orientations under the Taylor assumption of uniform strain (no interactions between neighboring grains).

The effect of polycrystallinity of the matrix phase on the mechanical response has also been examined. Compared to a single crystal matrix, a polycrystalline matrix results in: 1) higher stresses both macroscopically and in both phases; 2) an increase in the average stress and its standard deviation in the matrix phase; and 3) a decrease in the sensitivity to volume fraction (less variation in stress). In terms of strain rate, 1) more strain is accommodated in particles while less strain rate is taken up by matrix; 2) the average strain rate and its standard deviation decrease in the matrix phase; and 3) the sensitivity to volume fraction decreases (less variation in strain rate). In general, it can be concluded that microstructures with a polycrystalline matrix are less sensitive to changes in volume fraction, contiguity of particles, and microstructure type. This trend may be, however, not only a consequence of the polycrystallinity of the matrix in the microstructure, but also because of the change in texture of the matrix. Therefore, it is also of interest to examine the effect of texture of the matrix on the mechanical response

of the microstructure under uniaxial tension. This will be explored in a future publication.

Based on the full field information obtained, it becomes feasible to optimize microstructures for a certain preferred mechanical performance. For example, if the desired behavior is a more uniform strain rate in both phases, while minimizing the difference in average strain rates in the two phases, one can select the corresponding microstructure with a given particle volume fraction using Fig. 10. In other words, by varying the microstructural design of the material, a desired distribution of strain rate under uniaxial tension can be obtained. The material may be more resistant to failure in the form of local crack propagation or creep, for example. This is expected to be relevant to the optimization of microstructure in W-Ni-Fe heavy alloys (Churn and German, 1984), which motivated this investigation.

Even though the simulated microstructures show the characteristics expected from Ostwald ripening in liquid phase sintering, more microstructural characterizations such as two-point correlation functions (Rollett et al., 2007), particle shape analysis using a moment analysis (MacSleyne et al., 2008) and spatial distribution of particles using the k^{th} nearest neighbor analysis (Tong et al, 1999) should be performed on the simulated microstructures. The results could be compared with those from analysis of the real materials samples in order to verify the quality of the simulated microstructures. The analysis of the three-dimensional contiguity of particles during coarsening simulations with a fixed solid volume fraction showed a scale-variant characteristic such that, as the system coarsens, the contiguity of particles decreases. However, it was previously reported in the two-dimensional experimental study on WC-Co composites (Kim et al., 2008) that the contiguity of WC particles is scale-invariant with a given particle volume fraction. In other words, the microstructures attain a self-similarity in terms of the WC particle contiguity when measured in two-dimensional cross-sections. Note however that the WC particles in the system are highly faceted, in contrast to the approximately equiaxed particles considered in this work. These issues will be explored in the future.

Acknowledgements

Support from the User Productivity Enhancement and Technology Transfer Program (PET) of the High Performance Computing Modernization Office for S-BL and ADR is gratefully acknowledged. Conversations about composite materials with John Clayton and Tusit Weerasooriya of the Army Research Laboratory are gratefully acknowledged. The Intel Corporation is thanked for the provision of computing facilities. S-BL thanks Professor H-N Han for valuable conversations on the modeling of the plasticity.

References

Anderson, M.P., Grest, G.S., Srolovitz, D.J., 1985. Grain growth in 3 dimensions – A lattice model. Scripta Metall. 19(2), 225-230.

Anderson, M.P., Grest, G.S., Srolovitz, D.J., 1989. Computer simulation of normal grain growth in three dimensions. Phil. Mag. B. 59(3), 293-329.

Batra, R.C., Love, B.M., 2006. Consideration of microstructural effect in the analysis of adiabatic shear bands in a tungsten heavy alloy. Int. J. Plasticity 22, 1858-1878.

Becker, R., Panchanadeeswaran, S., 1995. Effects of grain interactions on deformation and local texture in polycrystals. Acta Metall. Mater. 43, 2701-2719.

Chawla, N., Ganesh, V.V., Wunsch, B., 2004. Three-dimensional microstructure visualization and finite element modeling of the mechanical behavior of SiC particle reinforced aluminum composites. Scripta Mater. 51, 161-165.

Chawla, N., Chawla, K.K., 2006. Microstructure-based modeling of the deformation behavior of particle reinforced metal matrix composites. J. Mater. Sci. 41, 913-925.

Chawla, N., Sidhu, R.S., Ganesh, V.V., 2006. Three-dimensional visualization and microstructure-based modeling of deformation in partile-reinforced composites. Acta Mater. 54, 1541-1548.

Churn, K.S., German, R.M., 1984. Fracture-behavior of W-Ni-Fe heavy alloys. Metall. Trans. A. 15A, 331-338.

German, R.M., 1985. The contiguity of liquid phase sintered microstructures. Metall. Trans. A. 16A, 1247-1251.

German, R. M., 1998. Powder Metallurgy of Iron and Steel. John Wiley & Sons, Inc.

Jernot, J.P., Chermant, J.L., 1982. On the importance of the contiguity and electrical-conductivity for sintered materials. Scripta Metall. 16, 943-946.

Kim, C.-S., 2004. Microstructural-Mechanical Property Relationship in WC-Co composites. Ph D. Thesis, Carnegie Mellon University.

Kim, C.-S., Massa, T.R., Rohrer, G.S., 2008. Interface character distributions in WC-Co Composites. J. Am. Ceram. Soc. 91(3), 996-1001.

Lebensohn, R.A., 2001. N-site modeling of a 3D viscoplastic polycrystal using fast Fourier Transform. Acta Mater. 49, 2723-2737.

Lebensohn, R.A., Brenner, R., Castelnau, O., Rollett, A.D., 2008. Orientation image-based micromechanical modeling of subgrain texture evolution in polycrystalline copper. Acta Mater. 56, 3914-3926

Fang, Z., Patterson, B.R., 1993. Experimental investigation of particle size distribution influence on diffusion controlled coarsening. Acta Metall. 41(7), 2017-2024.

Ganesh, V.V., Chawla, N., 2005. Effect of particle orientation anisotropy on the tensile behavior of metal matrix composites: experiments and microstructure-based simulation. Mater. Sci. Eng. A. 391, 342-353.

Gurland, J., 1966. An estimate of contact and contiguity of dispersions in opaque samples. Trans. Metall. Soc. AIME. 236, 642-646.

Lebensohn, R.A., Montagnat, M., Mansuy, P., Duval, P., Meysonnier, J., Philip, A., 2009. Modeling viscoplastic behavior and heterogeneous intracrystalline deformation of columnar ice polycrystals. Acta Mater. 57, 1405-1415.

Lee, S.-B., Rickman, J.M., Rollett, A.D., 2007. Three-dimensional simulation of isotropic coarsening in liquid phase sintering I: A model. Acta Mater. 55, 615-626.

Lifshitz, I.M., Slyozov, V.V., 1961. The kinetics of precipitation from supersaturated solid solutions. J. Phys. Chem. Solids. 19(12), 35-50.

Lin, P., Palumbo, G., Erb, U., Aust, K.T., 1995. Influence of grain boundary character distribution on sensitization and intergranular corrosion of alloy-600. Scripta Metall. Mater. 33, 1387-1392.

Liu, X., Hu, G., 2005. A continuum micromechanical theory of overall plasticity for particulate composites including particle size effect. Int. J. Plasticity 21, 777-799.

Llorca, J., Needleman, A., Suresh, S., 1991. An analysis of the effects of matrix void growth on deformation and ductility in metal-ceramic composites. Acta Metall. Mater. 39, 2317-2335.

MacSleyne, J.P., Simmons, J.P., De Graef, M., 2008. On the use of 2-D moment invariants for the automated classification of particle shapes. Acta Mater. 56, 427-437.

Matsushita, R., Senna, M., Kuno, H., 1977. Electrical-resistivity of hot-pressed silver-polystyrene powder mixture. J. Mater. Sci. 12, 509-516.

Mercier, S., Moinari, A., 2009. Homogenization of elastic-viscoplastic heterogeneous materials: Self-consistent and Mori-Tanaka schemes. Int. J. Plasticity 25, 1024-1048.

Michel, J.C., Moulinec, H., Suquet, P., 2000. A computational method based on augmented Lagrangians and fast Fourier Transforms for composites with high contrast. CMES-Comput. Mod. Eng. Sci. 1, 79-88.

Morawiec, A., Saylor, D.M., 1999. Registry between sections in precision sectioning of polycrystalline materials. ICOTOM-12, Montréal, Ottawa: NRC Res. Press, 198-203.

Moulinec, H., Suquet, P., 1994. A fast numerical method for computing the linear and nonlinear mechanical properties of composites. C. R. Acad. Sci. Paris II. 318, 1417-1423.

Moulinec, H., Suquet, P., 1998. A numerical method for computing the overall response of nonlinear composites with complex microstructure. Comput. Methods Appl. Mech. Eng. 157, 69-94.

Ostwald, W., 1900. Uber die vermeintliche Isomerie des roten und gelben Quecksilberoxyds und die Oberfiachenspannung fester Korper. Z. Phys. Chem. 34, 495-503.

Park, J.-K., Kang, S.-J.L., Eun, K.Y., Yoon, D.N., 1989. Microstructural change during liquid-phase sintering of W-Ni-Fe alloy. Metall. Trans. A. 20A, 837-845.

Patton, G., Rinaldi, C., Bréchet, Y., Lormand, G., Fougéres, R., 1998. Study of fatigue damage in 7010 aluminum alloy. Mater. Sci. Eng. A245, 207-218.

Pierard, O., Llorca, J., Segurado, J., Doghri, I., 2007. Micromechanics of particle-reinforced elasto-viscoplastic composites: Finite element simulations versus affine homogenization. Int. J. Plasticity 23, 1041-1060.

Ratke, L., Voorhees, P.W., 2002. Growth and Coarsening: Ripening in Matrieal Processing. Springer.

Rollett, A.D., Lee, S.-B., Campman, R., Rohrer, G.S, 2007. Three-dimensional characterization of microstructure by electron back-scatter diffraction. ARMR. 37, 627-658.

Rowenhorst, D.J., Kuang, J.P., Thornton, K., Voorhees, P.W., 2006a. Three-dimensional analysis of particle coarsening in high volume fraction solid-liquid mixtures. Acta Mater. 54(8), 2027-2039

Rowenhorst, D.J., Gupta, A., Feng, C.R., Spanos, G., 2006b. 3D crystallographic and morphological analysis of coarse martensite: combining EBSD and serial sectioning. Scripta Mater. 55, 11-16

Saylor, D.M., Morawiec, A., Rohrer, G.S., 2002. The distribution and energies of grain boundaries as a function of five degrees of freedom. J. Am. Ceram. Soc. 85, 3081-3083.

Saylor, D.M., El-Dasher, B.S., Adams, B.L., Rohrer, G.S., 2004. Measuring the five parameter grain boundary distribution from observations of planar sections. Metall. Mater. Trans. 35A, 1981-1989.

Shan, Z., Gokhale, A.M., 2001. Micromechanics of complex three-dimensional microstructure. Acta Mater. 49, 2001-2015.

Shen, Y.-L., Finot, M., Needleman, A., Suresh, S., 1994. Effective elastic response of two-phase composites. Acta Metall. Mater. 42, 77-97.

Srolovitz, D.J., Anderson, M.P., Grest, G.S., Sahni, P.S., 1983. Grain growth in 2 dimensions. Scripta Metall. 17, 241-246.

Suresh, S., 1998. Fatigue of Materials. Cambridge, UK: Cambridge Univ. Press: 617.

Tewari, A., Gokhale, A.M., 2001. Estimation of three-dimensional grain size distribution for microstructural serial sections. Mater. Characterization. 46, 329-335.

Tong, W.S., Rickman, J.M., Barmak, K., 1999. Quantitative analysis of spatial distribution of nucleation sites: Microstructural implications. Acta Mater. 47(2), 435-445.

Uchic, M.D., Groeber, M.A., Dimiduk, D.M., Simmons, J.P., 2006. 3D microstructural characterization of nickel superalloys via serial-sectioning using a dual beam FIB-SEM. Scripta Mater. 55, 23-28.

Underwood, E., 1970. Quantitative Stereology. New York: Addison-Wesley.

Vena, P., Gastaldi, D., Contro, R., 2008. Determination of the effective elastic-plastic response of metal-ceramic composites. Int. J. Plasticity 24, 483-508.

Fig 1 and Fig 2

Figure 1

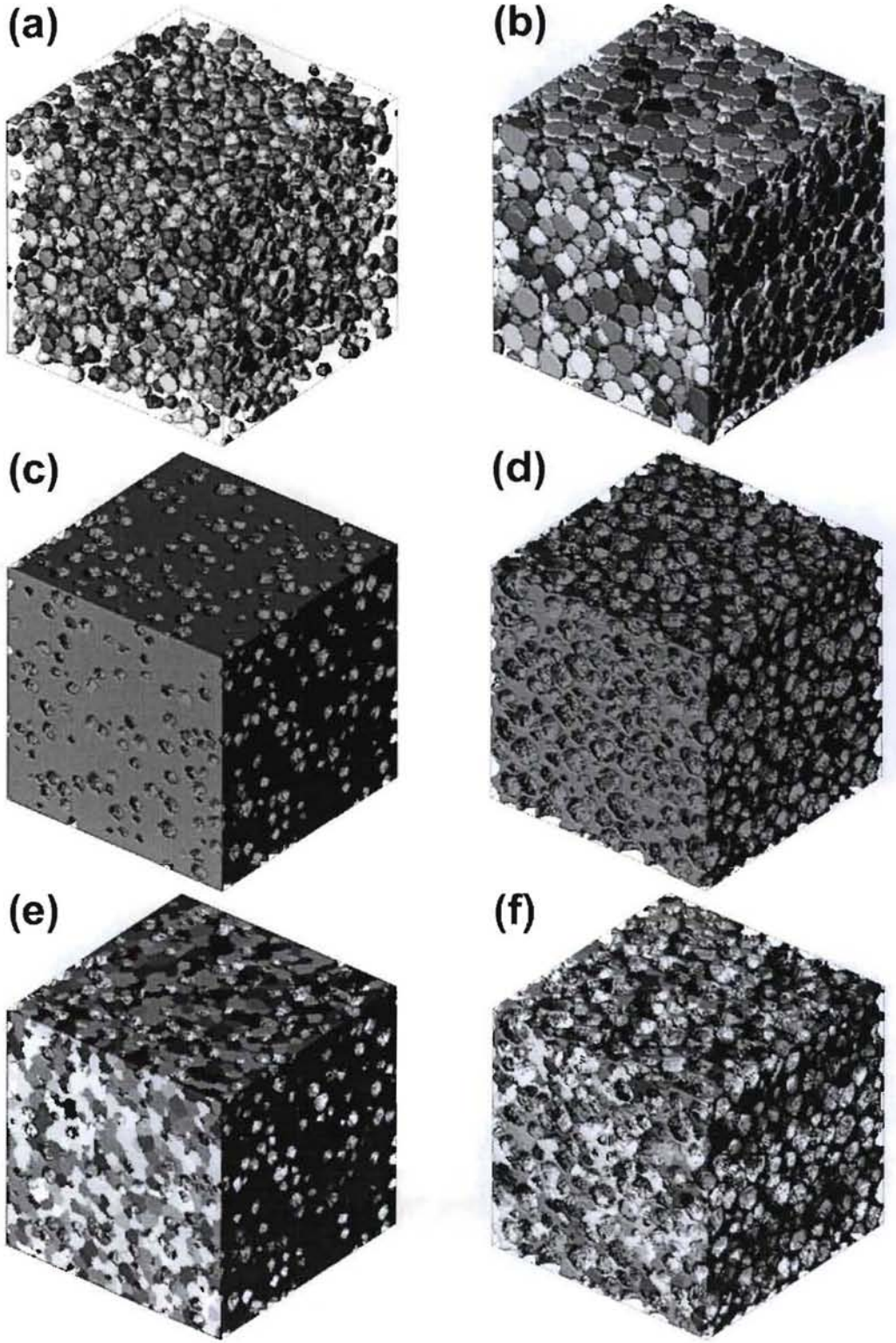

Figure 2

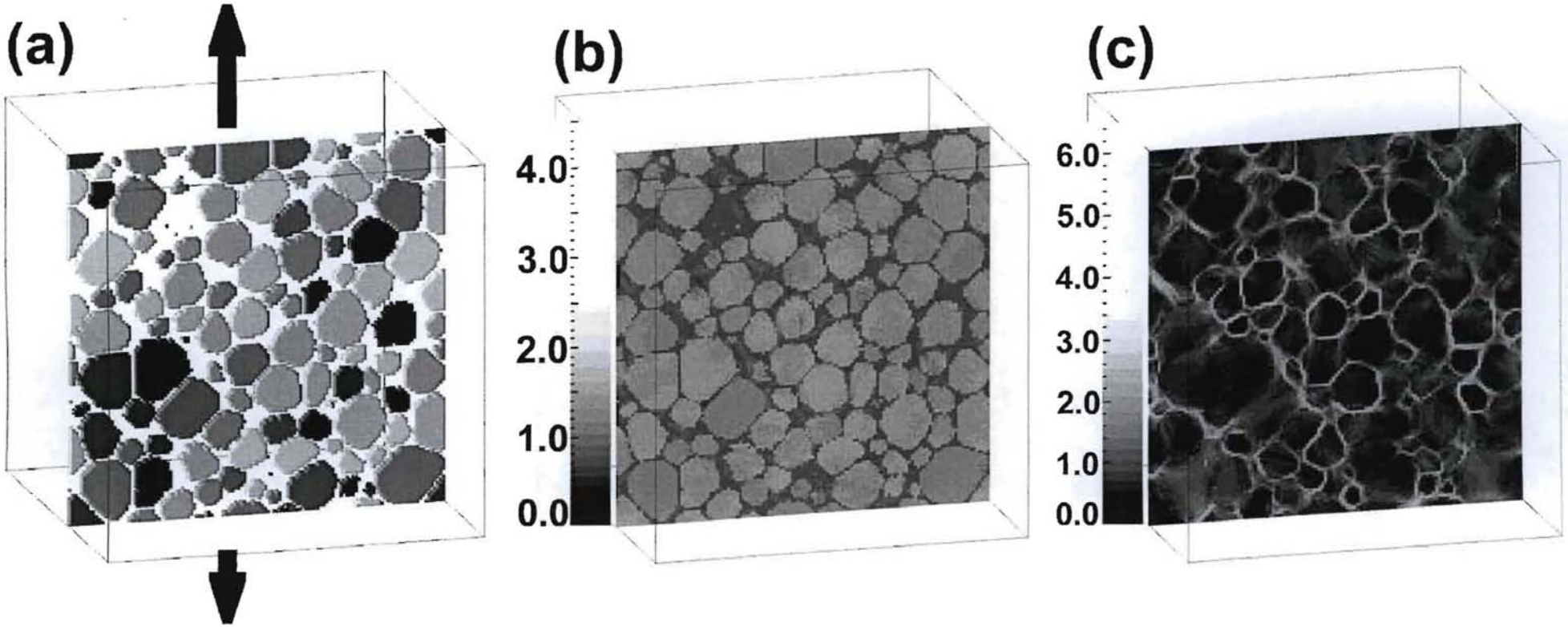

Fig 3 and Fig 4

Figure 3

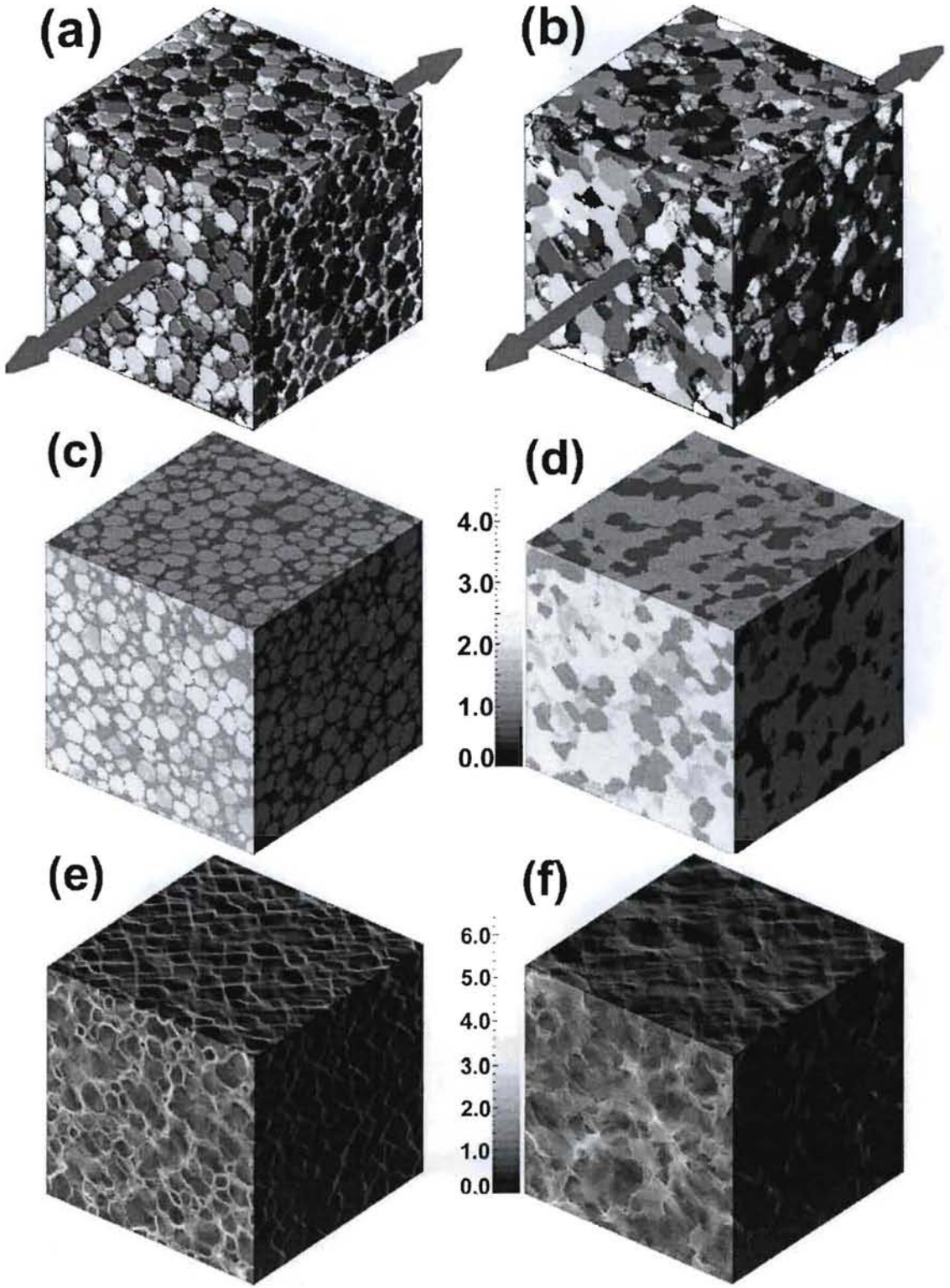

Figure 4

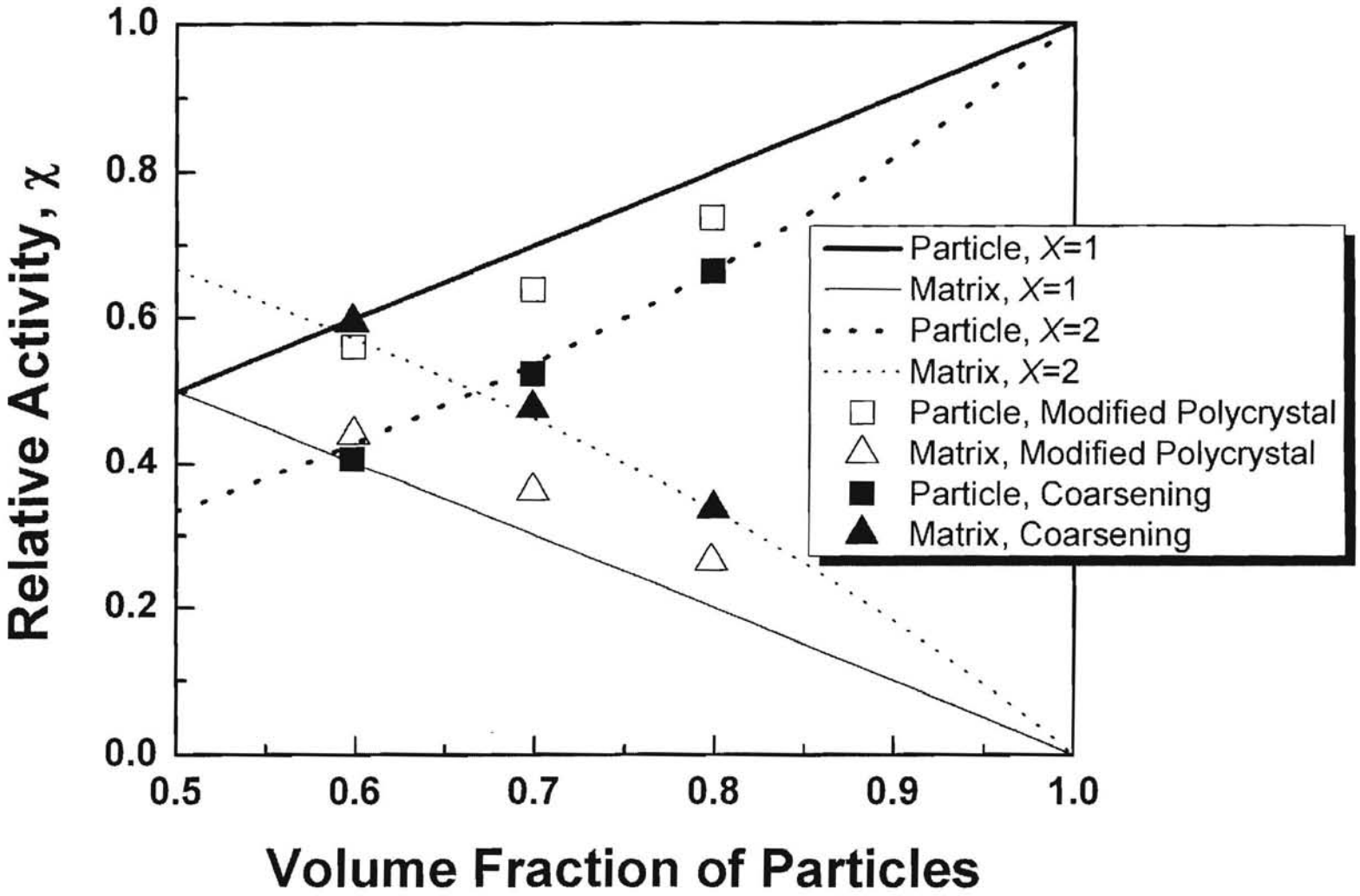
Relative Activity, χ
1.0
0.8
0.6
0.4
0.2
0.0
0.5
0.6
0.7
0.8
0.9
1.0
Volume Fraction of Particles
Particle, X=1
Matrix, X=1
Particle, X=2
Matrix, X=2
Particle, Modified Polycrystal
Matrix, Modified Polycrystal
Particle, Coarsening
Matrix, Coarsening

from Fig 5 and Fig 10

Figure 5

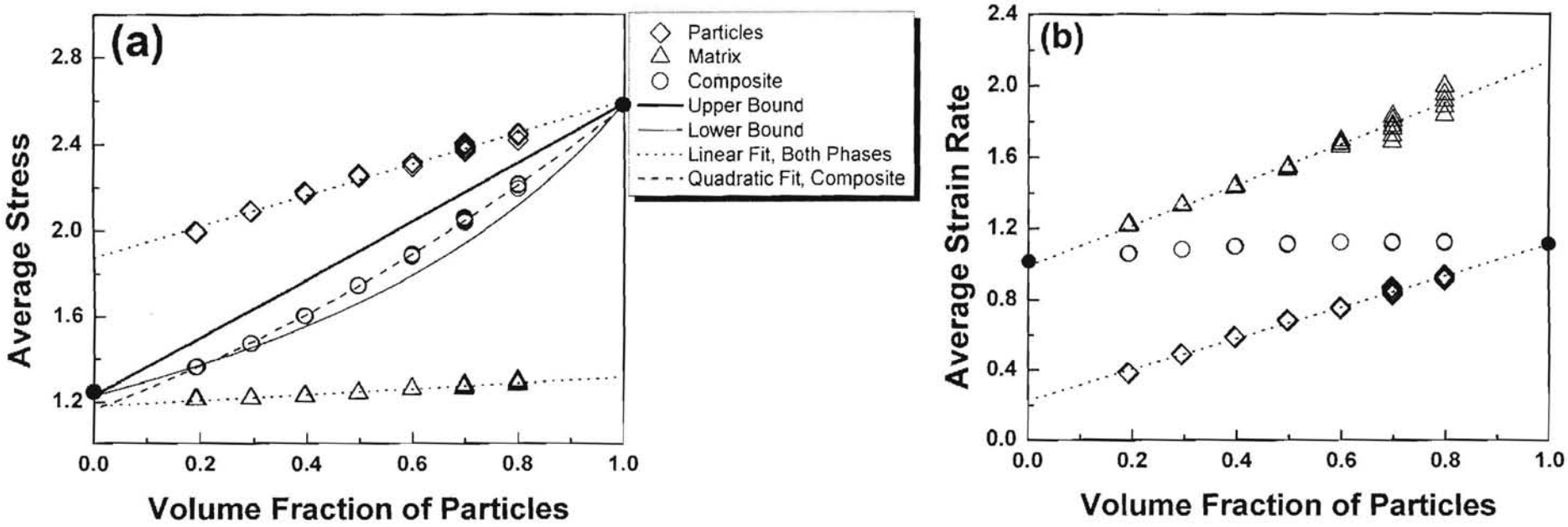

Figure 6

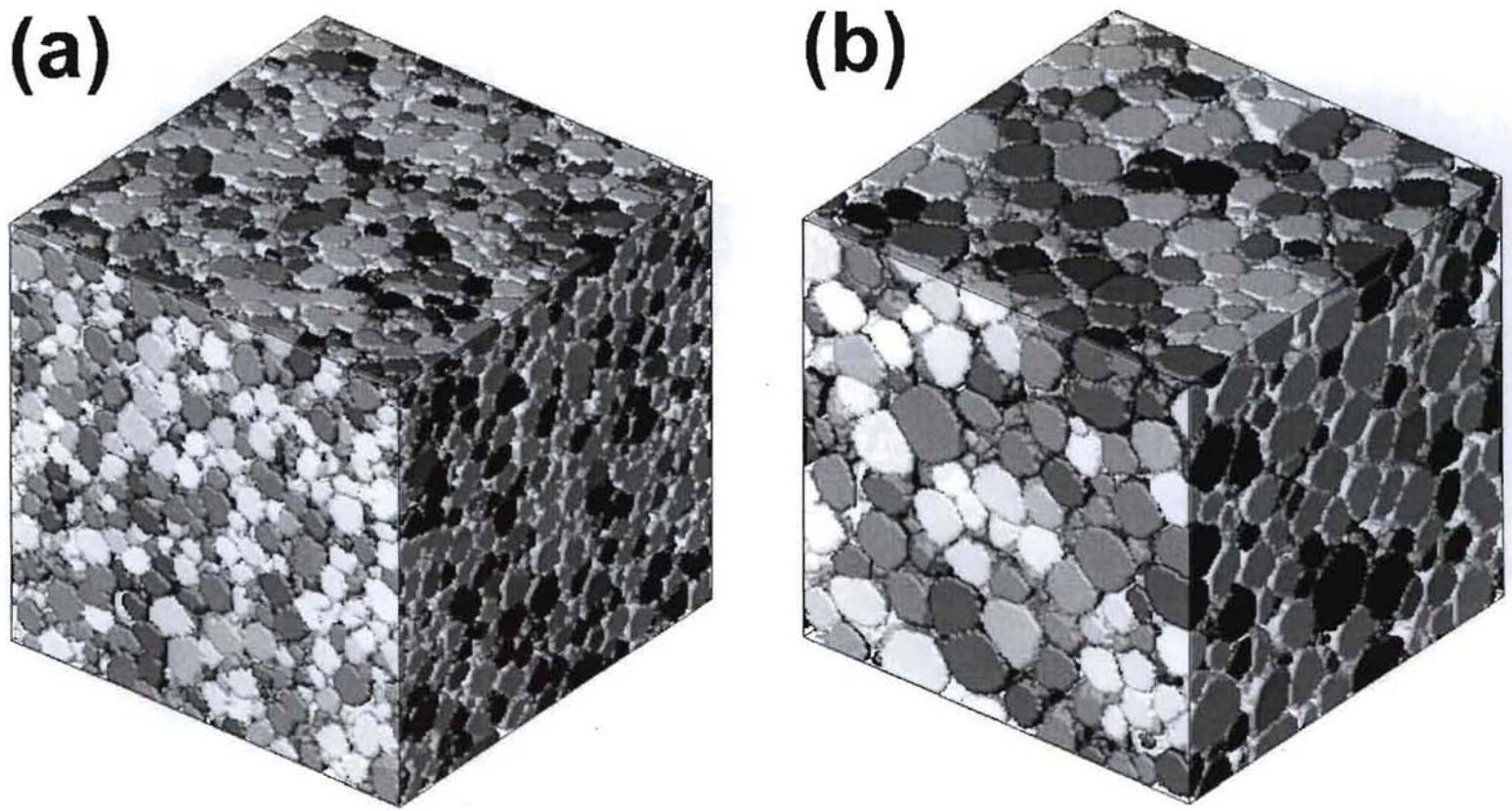

Figure 7

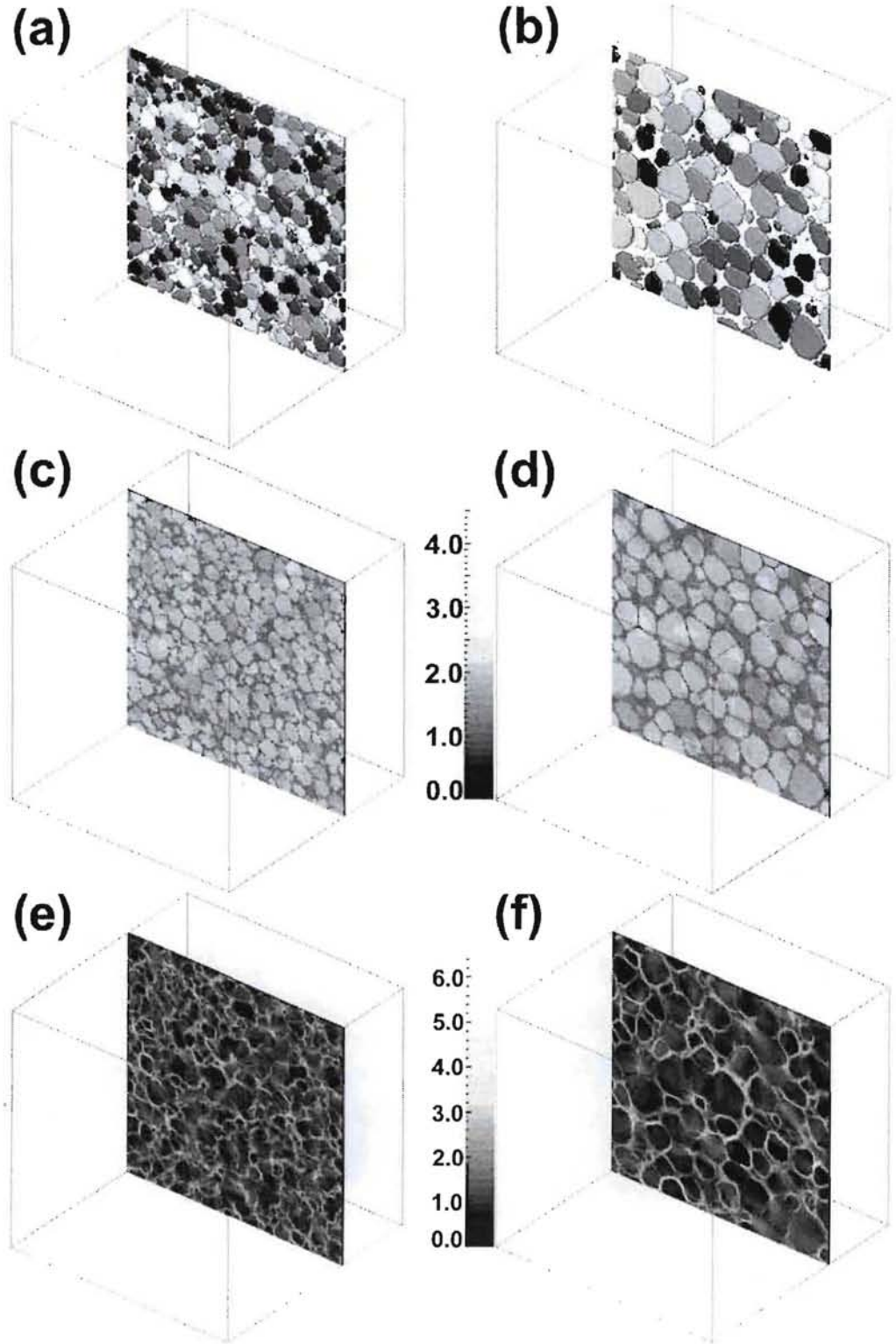

Figure 8

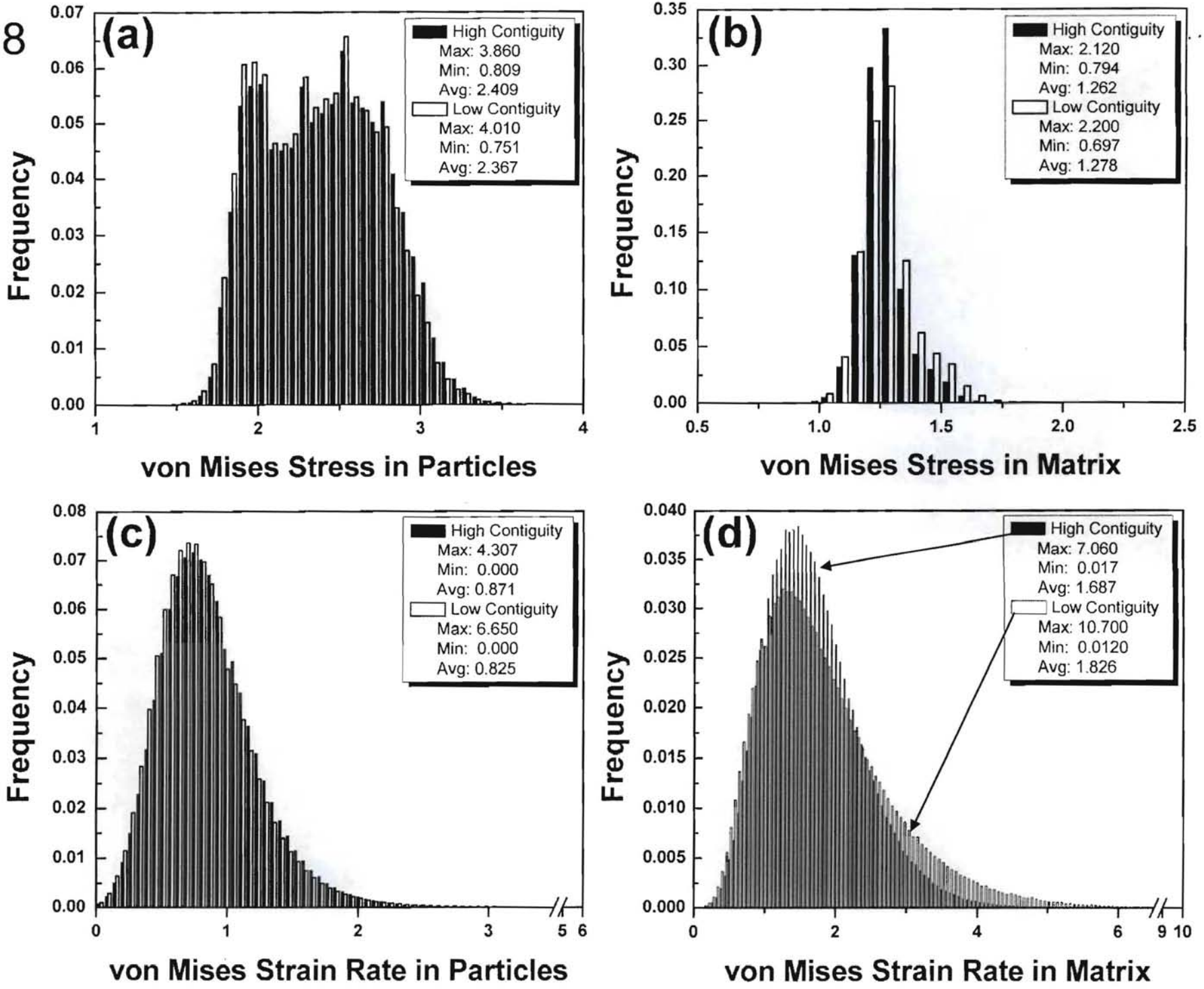
(a)
High Contiguity
Max: 3.860
Min: 0.809
Avg: 2.409
Low Contiguity
Max: 4.010
Min: 0.751
Avg: 2.367
Frequency
von Mises Stress in Particles
(b)
High Contiguity
Max: 2.120
Min: 0.794
Avg: 1.262
Low Contiguity
Max: 2.200
Min: 0.697
Avg: 1.278
Frequency
von Mises Stress in Matrix
(c)
High Contiguity
Max: 4.307
Min: 0.000
Avg: 0.871
Low Contiguity
Max: 6.650
Min: 0.000
Avg: 0.825
Frequency
von Mises Strain Rate in Particles
(d)
High Contiguity
Max: 7.060
Min: 0.017
Avg: 1.687
Low Contiguity
Max: 10.700
Min: 0.0120
Avg: 1.826
Frequency
von Mises Strain Rate in Matrix

Figure 9

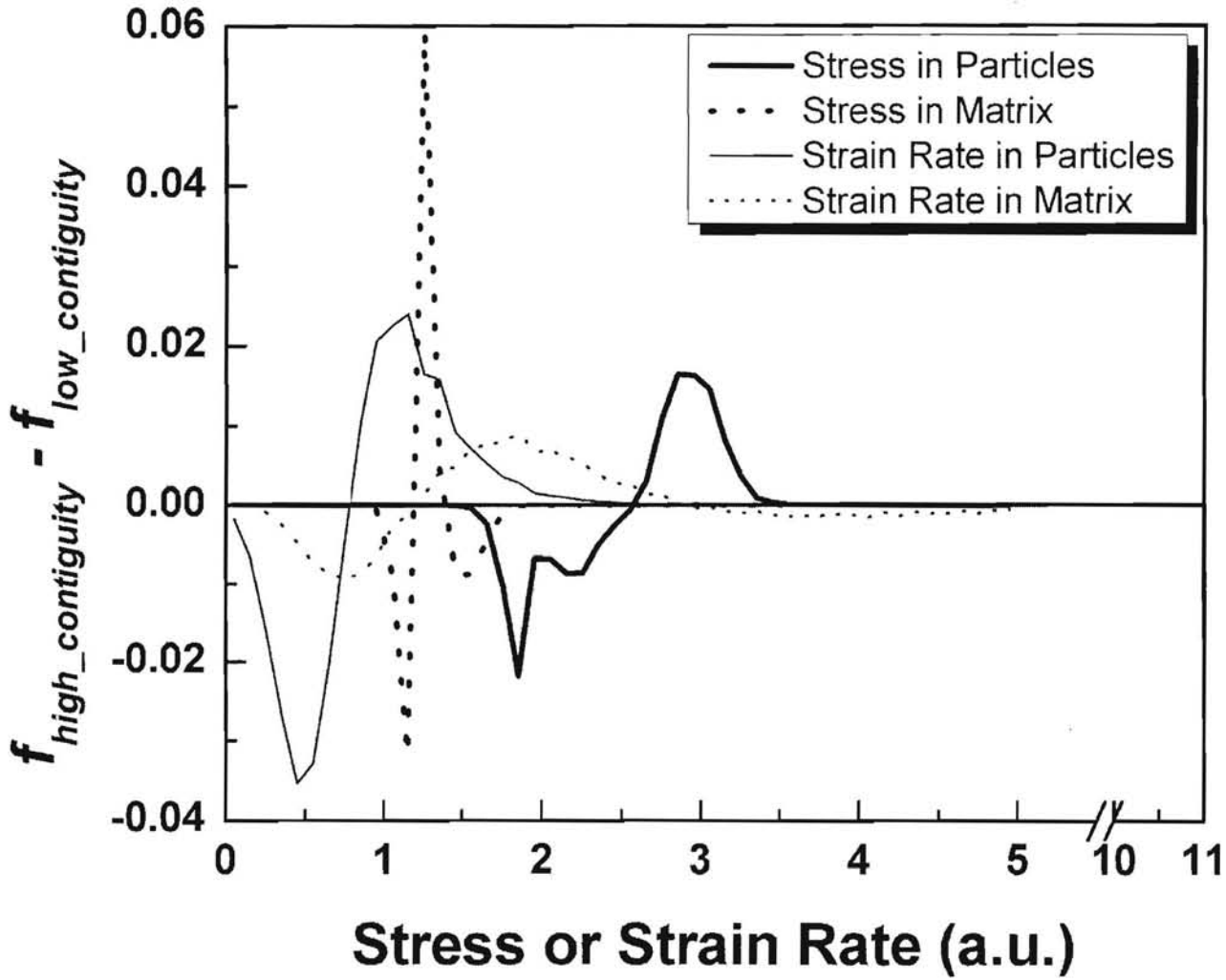
0.06
0.04
0.02
0.00
-0.02
-0.04
0
1
2
3
4
5
10
11
Stress in Particles
Stress in Matrix
Strain Rate in Particles
Strain Rate in Matrix
f high_contiguity - f low_contiguity
Stress or Strain Rate (a.u.)

Figure 10

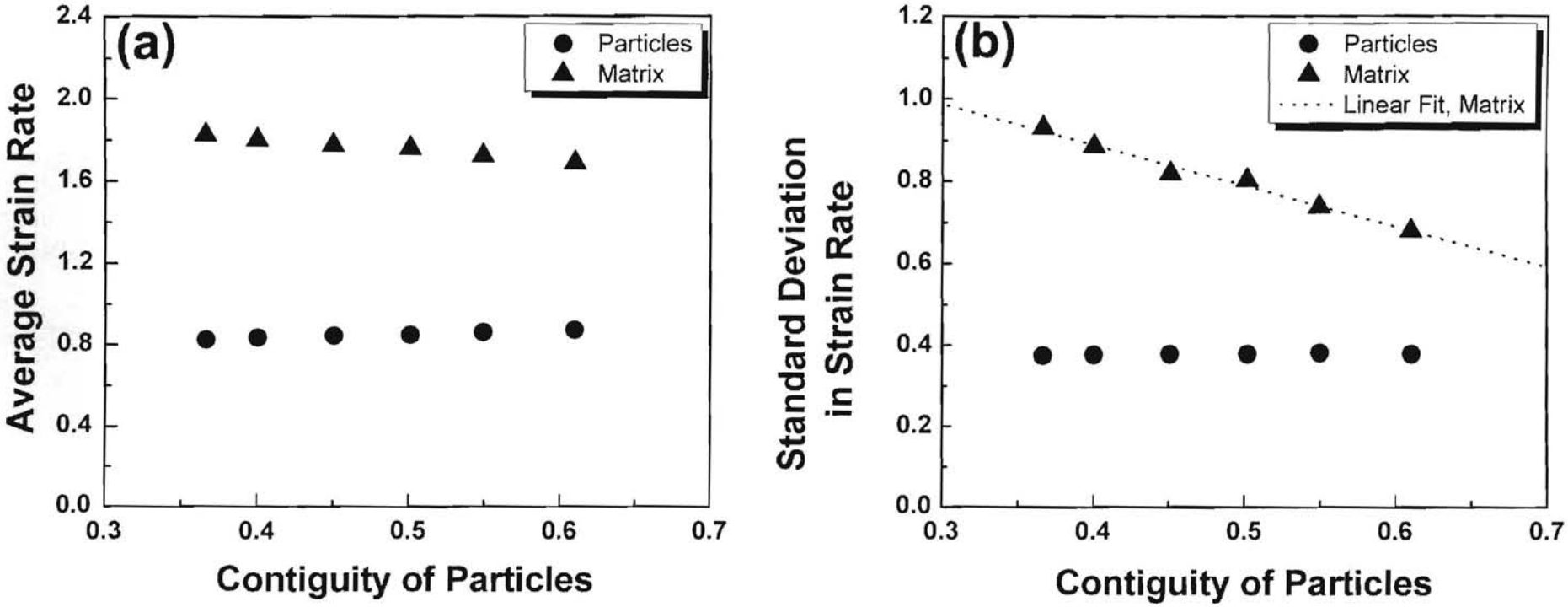
(a)
Particles
Matrix
Average Strain Rate
2.4
2.0
1.6
1.2
0.8
0.4
0.0
0.3
0.4
0.5
0.6
0.7
Contiguity of Particles
(b)
Particles
Matrix
Linear Fit, Matrix
Standard Deviation in Strain Rate
1.2
1.0
0.8
0.6
0.4
0.2
0.0
0.3
0.4
0.5
0.6
0.7
Contiguity of Particles

Figure 11

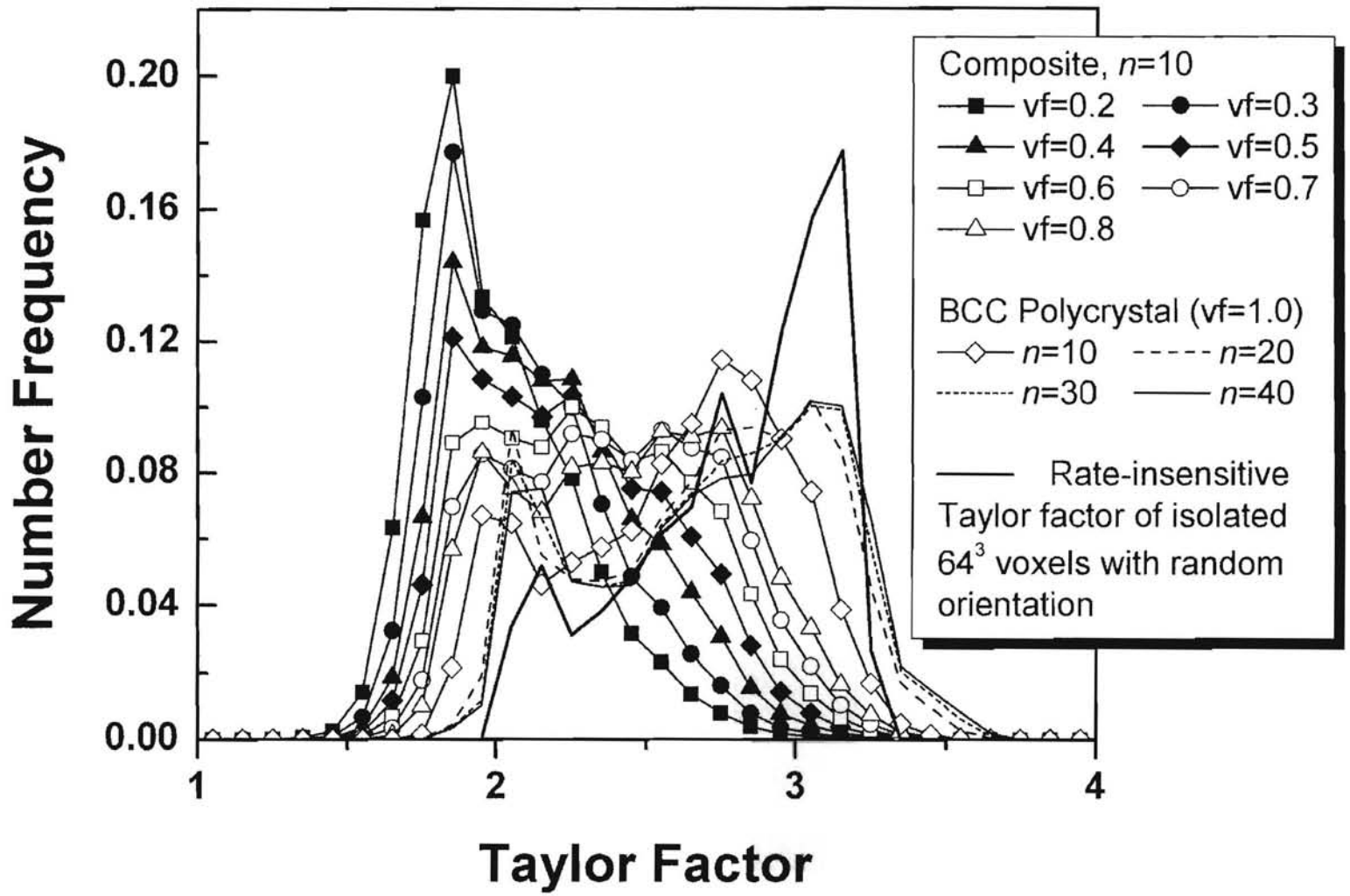
Number Frequency
0.20
0.16
0.12
0.08
0.04
0.00
1
2
3
4
Taylor Factor
Composite, n=10
vf=0.2
vf=0.3
vf=0.4
vf=0.5
vf=0.6
vf=0.7
vf=0.8
BCC Polycrystal (vf=1.0)
n=10
n=20
n=30
n=40
Rate-insensitive Taylor factor of isolated 64^3 voxels with random orientation

Figure 12

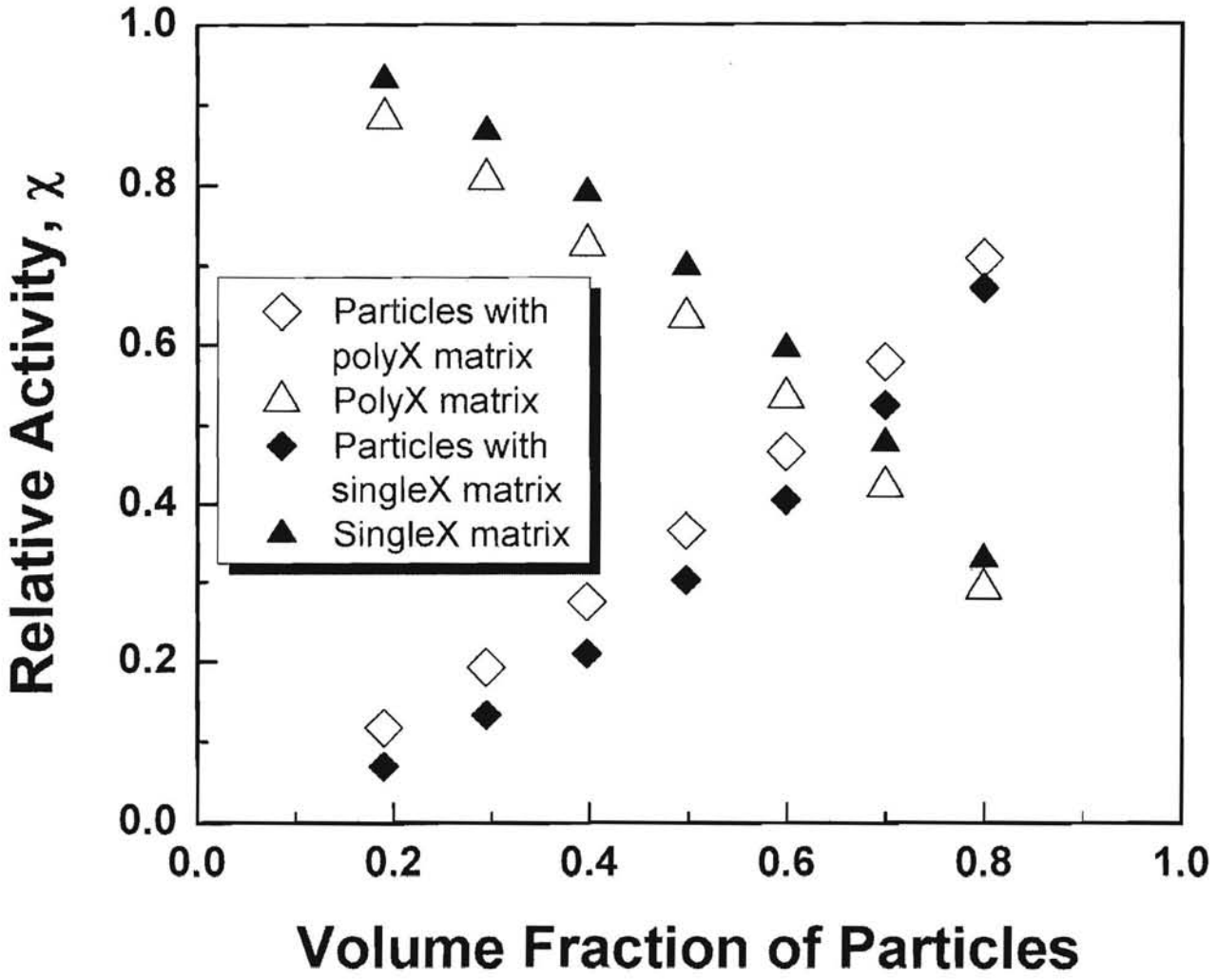
Relative Activity, χ
Volume Fraction of Particles
0.0
0.2
0.4
0.6
0.8
1.0
Particles with polyX matrix
PolyX matrix
Particles with singleX matrix
SingleX matrix

Figure 13

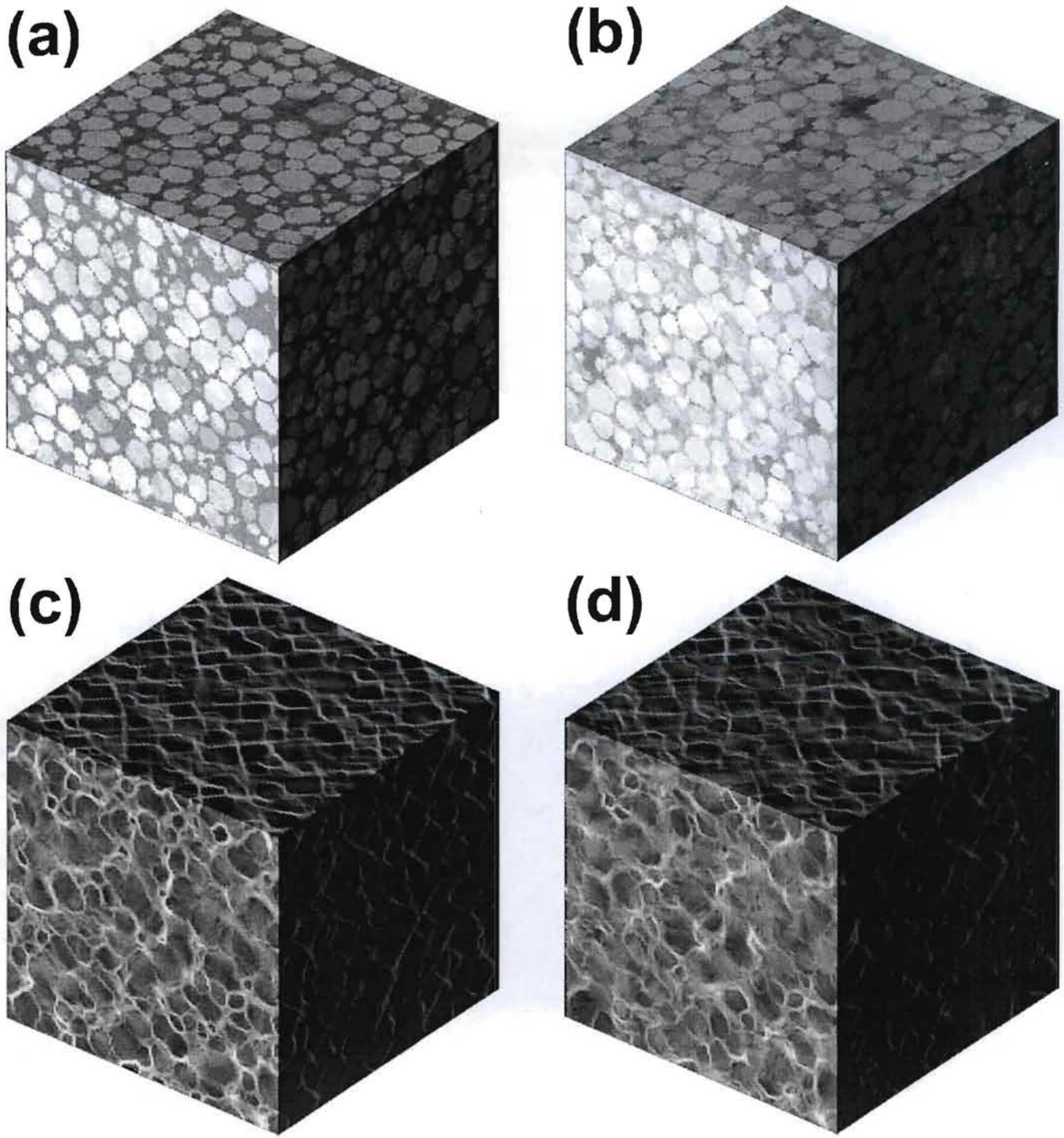

Figure 14

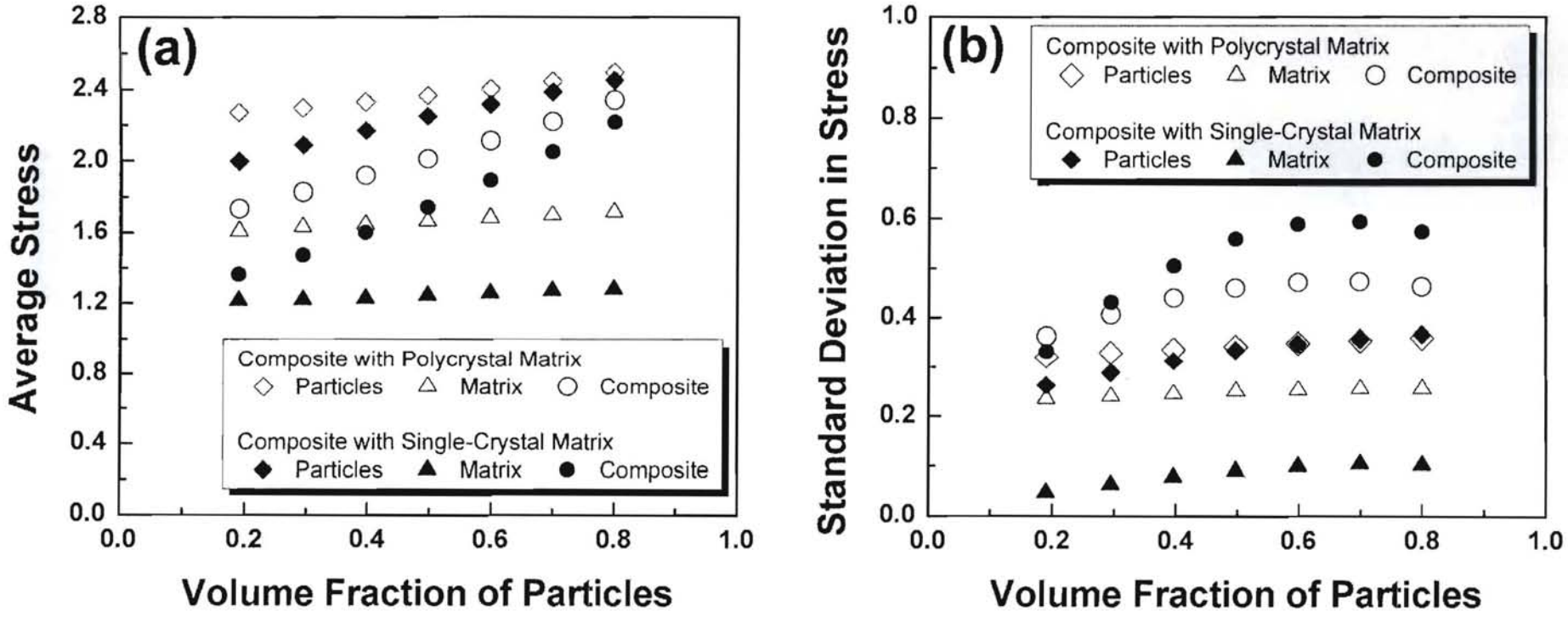
(a)
Average Stress
Volume Fraction of Particles
Composite with Polycrystal Matrix
Particles
Matrix
Composite
Composite with Single-Crystal Matrix
Particles
Matrix
Composite
(b)
Standard Deviation in Stress
Volume Fraction of Particles
Composite with Polycrystal Matrix
Particles
Matrix
Composite
Composite with Single-Crystal Matrix
Particles
Matrix
Composite

Figure 15

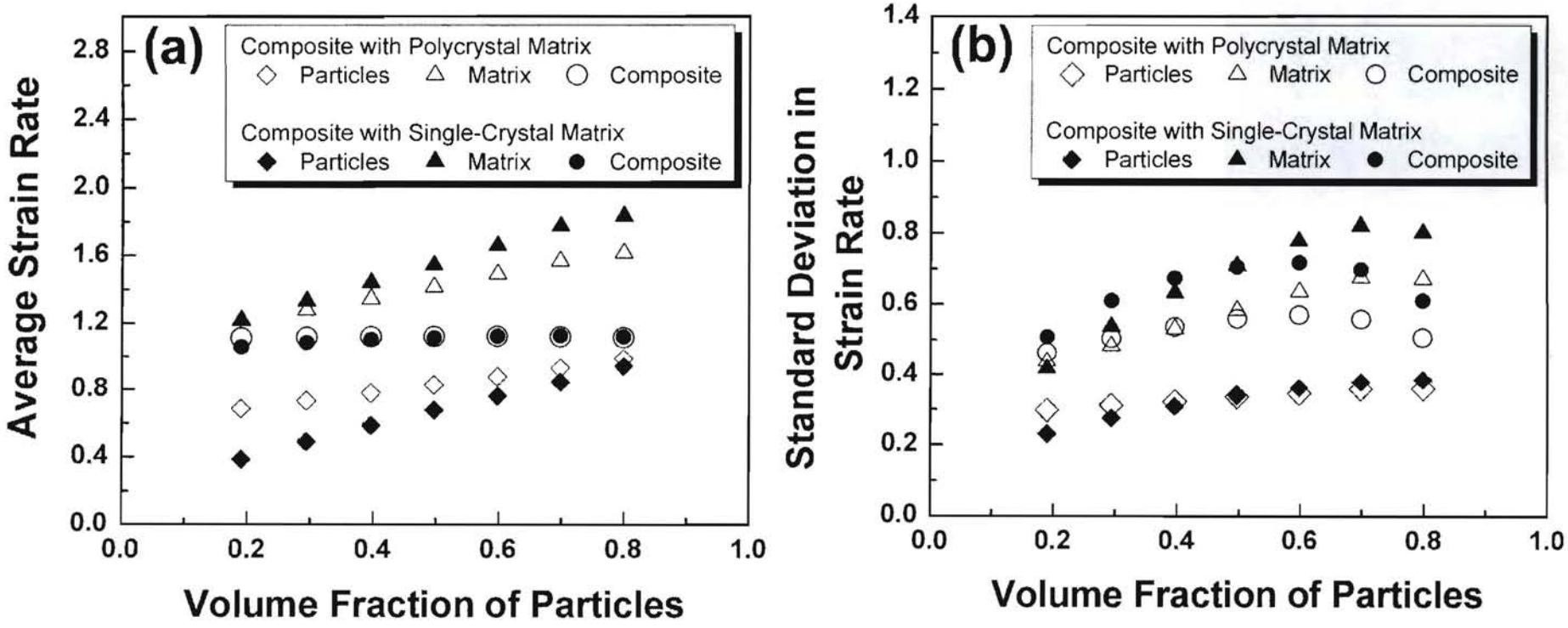
(a)
Composite with Polycrystal Matrix
Particles
Matrix
Composite
Composite with Single-Crystal Matrix
Particles
Matrix
Composite
Average Strain Rate
Volume Fraction of Particles
0.0
0.4
0.8
1.2
1.6
2.0
2.4
2.8
0.0
0.2
0.4
0.6
0.8
1.0
(b)
Composite with Polycrystal Matrix
Particles
Matrix
Composite
Composite with Single-Crystal Matrix
Particles
Matrix
Composite
Standard Deviation in Strain Rate
Volume Fraction of Particles
0.0
0.2
0.4
0.6
0.8
1.0
1.2
1.4
0.0
0.2
0.4
0.6
0.8
1.0

from Table 1 to Table 5

Table 1. Results from the property simulation on both the coarsened microstructure (Fig. 3(a)) and the "disordered" microstructure (Fig. 3(b)). Note that the difference in morphologies of two microstructures has a drastic influence on relative activities of the two phases.

	Coarsened Microstructure		Disordered Microstructure	
	Particle	**Matrix**	**Particle**	**Matrix**
# Particles	2029		2041	
Avg. Vol. Particles	618.32 (in voxel)		702.27 (in voxel)	
Particle Contiguity	0.2164		0.7987	
Volume Fraction	0.5982	0.4018	0.5988	0.4012
Macroscopic Stress of the composite	1.893 (in a.u.)		2.061 (in a.u.)	
Relative Activity	0.405	0.595	0.567	0.433

Table 2. The total number, the average volume and the contiguity of particles in both microstructures used as input for property simulations in terms of the volume fraction of particles. Note that "disordered" polycrystals have a much higher particle contiguity than the coarsened microstructures with fixed particle volume fraction and similar average volume of particles.

	Coarsened Microstructure			Disordered Polycrystal		
Particle Volume Fraction	0.6	0.7	0.8	0.6	0.7	0.8
# Particles	4058	4010	2406	4068	4418	2683
Avg. Vol. Particles	618.32	730.70	1393.43	698.61	704.80	1341.5
Particle Contiguity	0.2164	0.3786	0.5017	0.7955	0.8426	0.8805

Table 3. Results from the property simulation on both the coarsened microstructures with the same particle volume fraction (~0.7) but having different total number and contiguity of particles.

	Microstructure with High Particle Contiguity (0.5960)		Microstructure with Low Particle Contiguity (0.2443)	
	Particle	**Matrix**	**Particle**	**Matrix**
# Particles	4998		1002	
Volume Fraction	0.6974	0.3026	0.6988	0.3012
Macroscopic Stress of the composite	2.061 (in a.u.)		2.039 (in a.u.)	
Relative Activity	0.544	0.456	0.512	0.488

Table 4. Results of stress fields from the property simulation on both coarsened microstructures in Fig. 6 with the same particle volume fraction (~0.7) but different particle contiguities.

	Microstructure with High Particle Contiguity (0.5960)	Microstructure with Low Particle Contiguity (0.2443)
	Average Stress (in a. u.)	
Macroscopic	2.061	2.039 (-1.1%)
Particles	2.407	2.367 (-1.7%)
Matrix	1.262	1.278 (+1.3%)
	Standard Deviation in Stress (in a. u.)	
Macroscopic	0.611	0.584 (-4.4%)
Particles	0.366	0.354 (-3.3%)
Matrix	0.092	0.114 (+23.9%)

Table 5. Results of strain rate fields from the property simulation on both coarsened microstructures with the same particle volume fraction (~0.7, Fig. 6) but having different contiguity of particles.

	Microstructure with High Particle Contiguity (0.5960)	Microstructure with Low Particle Contiguity (0.2443)
	Average Strain Rate (in a. u.)	
Macroscopic	1.117	1.127 (+0.9%)
Particles	0.871	0.825 (-5.3%)
Matrix	1.685	1.826 (+8.4%)
	Standard Deviation in Strain Rate (in a. u.)	
Macroscopic	0.615	0.754 (-22.6%)
Particles	0.378	0.375 (-0.8%)
Matrix	0.679	0.930 (+37.0%)